SANDIA REPORT
SAND2001-1158
Unlimited Release
Printed July 2001

A Gas-Solid Riser Experiment for Fundamental Studies of Turbulent Multiphase Flow

Steven M. Trujillo, Kim A. Shollenberger, Timothy J. O'Hern, Thomas W. Grasser, and John R. Torczynski

Prepared by
Sandia National Laboratories
Albuquerque, New Mexico 87185 and Livermore, California 94550

Sandia is a multiprogram laboratory operated by Sandia Corporation, a Lockheed Martin Company, for the United States Department of Energy under Contract DE-AC04-94AL85000.

Issued by Sandia National Laboratories, operated for the United States Department of Energy by Sandia Corporation.

Available to DOE and DOE contractors from
U.S. Department of Energy
Office of Scientific and Technical Information
P.O. Box 62
Oak Ridge, TN 37831

Telephone: (865)576-8401
Facsimile: (865)576-5728
E-Mail: reports@adonis.osti.gov
Online ordering: http://www.doe.gov/bridge

Available to the public from
U.S. Department of Commerce
National Technical Information Service
5285 Port Royal Rd
Springfield, VA 22161

Telephone: (800)553-6847
Facsimile: (703)605-6900
E-Mail: orders@ntis.fedworld.gov
Online order: http://www.ntis.gov/ordering.htm

SAND2001-1158
Unlimited Release
Printed July 2001

A Gas-Solid Riser Experiment for Fundamental Studies of Turbulent Multiphase Flow

Steven M. Trujillo, Kim A. Shollenberger, Timothy J. O'Hern, Thomas W. Grasser
Thermal/Fluid Experimental Sciences

John R. Torczynski
Plasma, Aerosol and Noncontinuum Processes

Sandia National Laboratories
P.O. Box 5800
Albuquerque, NM 87185-0834

Abstract

The Multiphase Fluid Dynamics Research Consortium is funded by the U.S. Department of Energy Office of Industrial Technologies to combine industrial, academic, and National Laboratory research capabilities to improve modeling capabilities for turbulent gas-solid flows. Sandia's role in the consortium is the development of a gas-solid riser experiment, development and implementation of diagnostics, and acquisition of experimental data in support of model-development efforts. This report describes the experimental testbed, the associated diagnostics implemented at present, and representative data sets.

Acknowledgements

Construction and modifications to the riser, its subsystems and diagnostics reflect the skilled contributions of Rocky J. Erven and John J. O'Hare; we extend our thanks to them for their work. We are also grateful to MFDRC member personnel for their technical advice in the development of the riser facility, particularly Ray Cocco (Dow Chemical), Paul Merz and Charlie Guthrie (Chevron), Wen-Ching Yang (Siemens-Westinghouse), Ted Knowlton (PSRI), Rutton Patel (Exxon-Mobil), Sankaran Sundaresan (Princeton University), and Herb Weinstein (City College of New York). Formation of the MFDRC was spearheaded by Tyler Thompson (Dow Chemical); his support and enthusiasm are appreciated. The MFDRC is funded by the DOE Office of Industrial Technologies, under the direction of Brian Valentine. Finally, Arthur C. Ratzel's leadership is gratefully acknowledged.

Contents

1. Introduction 8
2. Riser Component Design and Construction 10
3. Original Riser Configuration 14
4. Modified Riser Configuration 17
5. Extended Riser Configuration 19
6. Triboelectric Effects 21
7. Mass Flux Diagnostics Development 23
7.1 Mass Flux Measurement by Porous Valves 24
7.2 Mass Flux Measurement by Suction Probes 30
8. Particle Diagnostics 35
9. Other Diagnostics and Future Work 38
References 40

Figures

Figure 1 – Schematic diagram of generic riser configuration. 8
Figure 2 – Drawing of Sandia riser disengagement section 12
Figure 3 – Drawing of Sandia riser engagement section. 13
Figure 4 – Original Sandia riser configuration. 14
Figure 5 – Differential pressure traces in (a) the riser, and (b) the downcomer. The downcomer pressure trace reflects the behavior of the surface of the bed within the measurement section. 16
Figure 6 –Sandia riser after flow-loop modifications. 18
Figure 7 – Differential pressure traces in (a) the riser and (b) the downcomer for the configuration shown in Figure 6. The downcomer pressure trace reflects the behavior of the surface of the bed within the measurement section. 19
Figure 8 – Sandia riser configuration after extension through Building 865 roofline 21
Figure 9 – Detail of humidification system as installed in air supply line, showing original and modified spray cone angles. 22
Figure 10 – Detail of disengagement-to-downcomer standpipe showing location of porous valve installation for mass-flux measurement 25
Figure 11 – Differential pressure trace in downcomer indicating height of bed surface during porous-valve closures for mass flux determination: (a) complete time history in which each negative Δp spike corresponds to a porous-valve closure; (b) trace for a single porous-valve closure, showing application of linear curve fit to determine mass flux from rate of bed-height decrease. 26
Figure 12 – Differential pressure traces in downcomer indicating height of bed surface during porous-valve closures in 50%-solids-metering case. 27
Figure 13 – Effect of fit domain on estimates of mass flux from differential pressure traces in Figure 11 28
Figure 14 – Differential pressure traces in riser sections during 10- and 20-second porous-valve closures for 50%-solids-metering case. Traces are offset so that time

$t = 0$ corresponds to the valve closure time. Pressures measured across sections spanning (a) $0.8 \le z_r/D_r \le 2.9$ (b) $7.3 \le z_r/D_r \le 9.5$, and (c) $18.2 \le z_r/D_r \le 20.4$. "Mean" line indicates time-mean of Δp with porous valve open. 29
Figure 15 – Schematic diagram of Sandia flux probe system. 31
Figure 16 – Drawing of 9.53-mm OD, 7.37-mm ID flux probe 31
Figure 17 – Flux probe measurements in the riser at $z_r/D_r = 17$. (a) probe inserted from side of riser opposite particle entry to engagement section; (b) probe inserted from same side as particle entry. 33
Figure 18 – Proposed explanation of bias mechanism in downbound near-wall flux probe samples. (a) particle concentration at probe tip in downbound sampling position. (b) probe self-shielding in upbound sampling position 34
Figure 19 – Flux probe measurements in the riser at $z_r/D_r = 17$; probe inserted from same side as particle entry to engagement section 35
Figure 20 – Microphotograph of FCC catalyst before loading into the Sandia riser; photo dimensions are approximately 1000 microns horizontal × 500 microns vertical. 36
Figure 21 – Microphotograph of FCC catalyst collected from the Sandia riser bag house after nominally 10 hours of running; photo dimensions are approximately 1000 microns horizontal × 500 microns vertical. 36
Figure 22 – Volumetric size distributions for two samples of fresh FCC catalyst used in the Sandia riser 37
Figure 23 – Volumetric size distributions for two samples of FCC catalyst collected from the Sandia riser bag house. 37
Figure 24 -- Schematic of gamma-densitometry tomography (GDT) system in the horizontal plane 39

Tables

Table 1 – MFDRC Structure: Partners and contributed expertise. 10

Nomenclature

Greek

ρ	mass density, kg/m^3

Roman

A	area, m^2
D	diameter, m
G	mass flux, $kg/m^2 \cdot s$
g	gravitational acceleration, m/s^2
h	height, m
p	pressure, Pa
R	radius, m
r	radial coordinate, m
t	time, s
U	velocity, m/s
z	axial coordinate, m

Subscripts

c	cross-sectional
g	gas
p	particle
r	riser
s	solids

1. Introduction

Multiphase interactions are central to many common processes in the chemical and petroleum industries. Gas-solid interactions occur in vertical columns of co-flowing gas and solids; such reactors are known as "risers" and are the reactor system of choice in certain specialized but important applications. Foremost among these are the fluidized catalytic cracking of hydrocarbons into higher-order petroleum products (the so-called "FCC" process) and pulverized coal combustion. A typical riser flow loop, omitting reaction-specific components, is shown schematically in Figure 1. Particles are fed from a storage and/or return leg, known as a "downcomer," into the riser itself. There, they are mixed with the transport gases and travel upward through the riser column. At the top of the riser, the particles and gas are separated, typically through multiple stages of cyclone separators. The gas continues to its next destination, and the particles are returned to the downcomer, where they are recycled through the flow. The gas flow in the riser is thus typically single-pass in nature, while the particle flow is multiple-pass. As a result, riser reactors are also known as "circulating fluidized beds" (CFBs).

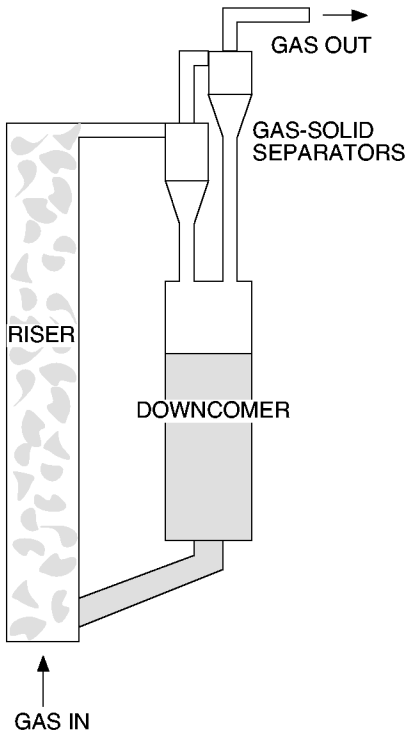

Figure 1 – Schematic diagram of generic riser configuration.

Despite their acceptance in industrial application, riser reactors are relatively problem-prone. A Rand Corporation study (Merrow, 1986) found that solids processing facilities in the petrochemical industries suffer from an average 37% performance shortfall relative to their design efficiencies; the average shortfall for non-solids plants was only 16%, and typical industry goals are 5-10% shortfall. The reduced performance in the solids-processing plants was linked very strongly to physical and mechanical solids-flow difficulties and linked only weakly to problems with the intended process chemistry. It should be noted that Merrow's study was not limited to CFB units but examined a wide range of solids-intensive operations; however, "hard" CFB unit reliability data are scarce, and the complications introduced to any generic process step by the addition of solids to the process stream are relatively common across processes.

The immense scale of the economy in which such reactors operate must also be borne in mind when considering industrial-scale reaction facilities. It is easy to estimate from typical reactor data that a sustained fractional-percentage increase in hydrocarbon-processing riser reactor efficiency would result in the economic benefit of millions of barrels of increased annual product yield and the ecological benefit of a reduced waste stream. Thus, even small but consistent process improvements are eagerly sought.

Typical riser design work involves an interaction between chemists and chemical engineers, with the former designing the reaction and the latter developing the ability to carry it out profitably at a large scale. Construction proceeds through a series of non-reacting ("cold-flow") and reacting models of increasing size and complexity, each one going through a development and troubleshooting phase, at costs that routinely run into millions of dollars. A major source of the difficulty in riser design is the inability to accurately predict the hydrodynamics of riser operation. Even when operated with no particles, the gas flow in the riser is turbulent and is thus difficult to predict in any spatial or temporal detail other than by computational means. However, the addition of solid particles to the flow at volumetric concentrations as high as 40% renders the equations of motion even more complex and intractable.

To address the need to develop the ability to computationally model gas-solid flows inexpensively and reliably, the Multiphase Fluid Dynamics Research Consortium (MFDRC) was organized in the spring of 1998. In this unique cooperative effort, companies have agreed to work toward the specific, mutually beneficial goals of improved modeling of riser and spouting-bed gas-solid flows (spouting-bed flows are a second type of gas-solid flow, typified by gas passing through a bed of non-circulating solids). Besides corporate members, the MFDRC includes the efforts of academic researchers and, through the U.S. Department of Energy (DOE) Office of Industrial Technologies (OIT), the support of five National Laboratories. The MFDRC is a pre-competitive partnership: all partners share the results equally, and none of the data are considered proprietary. The MFDRC membership structure is shown in Table 1.

Industry	Industrial Experience	Modeling & Simulation	Facilities & Equipment	Diagnostics Development
AEA Technology		○		
Chevron Research & Technology	○	○		
Dow Chemical	○	○		○
Dow Corning	○	○		
Du Pont	○	○		
Exxon Research & Engineering	○	○	○	
Fluent, Inc.		○		
Millennium Inorganic Chemicals	○	○		
Particulate Solid Research, Inc.	○			
Siemens Westinghouse	○		○	
Silicon Graphics, Inc.		○		
Academia				
Clarkson University		○		
Illinois Institute of Technology		○		○
Princeton University		○		○
Purdue University		○		○
The University of Colorado at Boulder		○		
The University of Michigan				○
Washington University at St. Louis				○
National Laboratories				
Los Alamos		○		
National Energy Technology Laboratory		○	○	
Oak Ridge		○	○	
Pacific Northwest			○	○
Sandia		○	○	○

Table 1 – MFDRC Structure: Partners and contributed expertise.

The role of Sandia National Laboratories in the MFDRC is to develop an experimental riser facility for the generation of high-quality data to be used in validating the computational models developed by MFDRC members. Additionally, Sandia is developing some of the diagnostic tools used to obtain these data sets and is coordinating the development and implementation of diagnostics developed outside Sandia. The intent of this document is to provide a brief summary of Sandia's efforts in connection with the development and operation of the MFDRC riser.

2. Riser Component Design and Construction

The riser configuration was designed by Sandia Department 9112 (Thermal/Fluid Experimental Sciences) personnel with the assistance of MFDRC partners. Because the focus of the consortium is hydrodynamics and not chemical kinetics, the Sandia riser was

designed as a cold-flow unit. The Engineering Sciences Experimental Facility (ESEF; Building 865) was chosen for facility construction for several reasons: suitable high-bay space was available in the building; the presence of the trisonic and hypersonic wind tunnels in the building ensured that a large supply of compressed air was available for use as motive and auxiliary air; and the managerial aspects of the building itself fell under Department 9112's leadership, streamlining the administrative processes that accompany a new, large-scale experiment.

The mission of diagnostics development was a critical design driver, demanding a design that would easily accept the installation of unspecified diagnostics. For the riser itself, a modular design was adopted, using identical 61-cm-long sections. Each section is fitted with a selection of 6.35- and 12.7-mm ports for the installation or insertion of probes. The sections mate using standard Schedule-80 PVC flange connections. This modularity allows the later fabrication and insertion of entire diagnostic-specific sections, if necessary, with little down-time. The downcomer design was similarly modular, using 61- and 122-cm acrylic sections and Schedule-80 PVC flange connections. The riser inner diameter of 14 cm was chosen to be as compact as possible, minimizing overall facility size, while meeting most industrial guidance recommending minimum test-unit sizing for acquisition of data that may be reliably applied to full-scale facilities. The downcomer inner diameter of 28 cm was chosen to create a solids reservoir that could accommodate a wide range of operating conditions.

To reduce construction time and costs, off-the-shelf parts in standard sizes were used whenever possible. Two critical fabricated parts were the stainless steel engagement section at the base of the riser and the large (58-cm ID) disengagement chamber at the top of the riser. Structural analyses of these parts were performed at Sandia by personnel in Department 6215 (Solar Thermal Test). The riser also incorporated parts donated by Westinghouse Corporation as part of the MFDRC, notably the riser support structure, cyclone separators, and the screw feeder and storage hoppers used in the original system configuration, described below.

Particular attention was devoted to the design of the disengagement section, in which the riser flow terminates and in which, in the Sandia design, the majority of air-particle separation is effected. A shortcoming seen in most published riser research is that the effects of asymmetries in riser termination (typically a 90° elbow) and in air-particle disengagement propagate upstream and affect the riser flow itself. To overcome this, a large, axisymmetric termination and disengagement chamber was designed. Several concepts were developed and analyzed by MFDRC partners at Los Alamos National Laboratory. The final selection is shown in Figure 2. The riser flow enters the disengagement co-axially and terminates at a penetration height of 61 cm. The air-particle mixture is impacted on an aluminum plate to separate the particles, which settle into an annular fluidized bed at the base of the disengagement section. This fluidized bed in turn empties into the downcomer via an underflow standpipe. The motive air, with any remaining particles, exits through two holes at the top of the chamber.

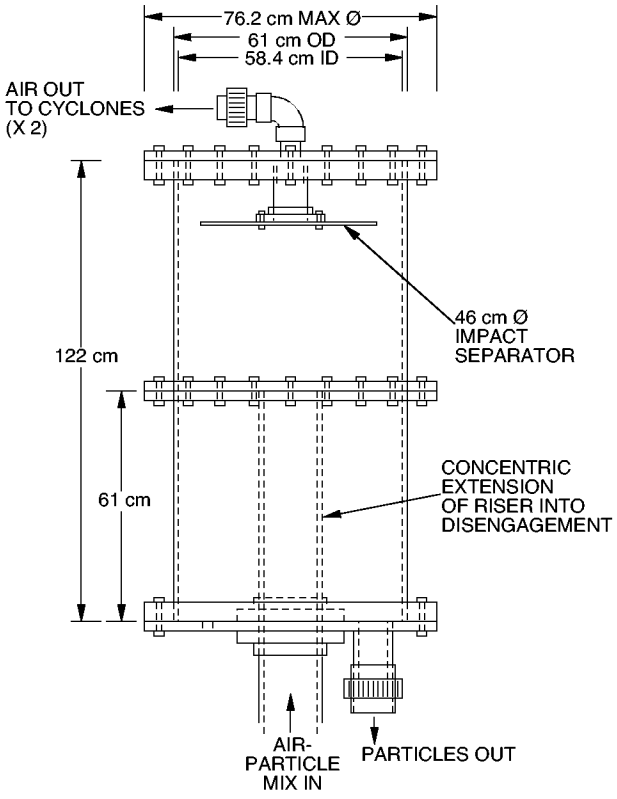

Figure 2 – Drawing of Sandia riser disengagement section.

Symmetry concerns were also addressed in the design of the engagement section, in which particles and motive air are mixed before entering the riser. The annular design shown in Figure 3 was chosen. Particles enter the engagement section via an angled standpipe and form a bed which is fluidized by a ring of eight equally-spaced ports (ports not shown in Figure 3). The motive air inlet pipe enters vertically through the bed's center; motive air thus entrains particles from the fluidized bed and transports it up the riser. The engagement section was built of ANSI-standard stainless steel pipe sections and was fabricated by personnel in Department 6215.

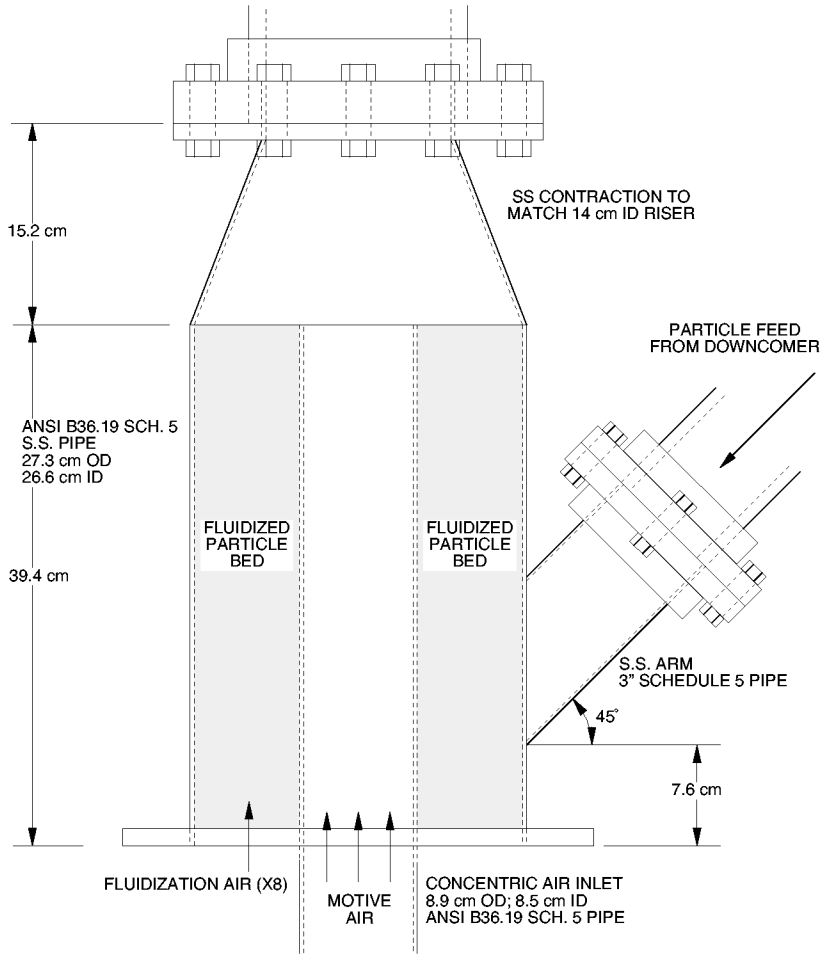

Figure 3 – Drawing of Sandia riser engagement section.

Baseline diagnostics and controls incorporated into the initial riser design were pressure measurements around the flow loop, fluidization-air control and metering at several locations in the loop, and manual-valve control and orifice metering of the motive air supply. Pressure-measurement and fluidization-air-injection ports were protected from catalyst contamination by flush-mounted sintered metal disks of 10-micron pore size. Pressure measurements were made using Validyne™ differential pressure transducers (DP15 family) with 5 kHz excitation. Transducer ranges were matched to local conditions. Transducer accuracy is ±0.25% full scale. All diagnostics were integrated into a set of PC-based LabView™ data acquisition programs; data were acquired at nominally 3 Hz. Some on-line data presentations were implemented, with complete data sets available for post-processing.

3. Original Riser Configuration

The original riser system layout is shown in Figure 4. In this configuration, solid particles flowed from the downcomer through an angled standpipe into the engagement section, described above. Particle flow rate in the loop was controlled by a manually-actuated knife valve at the base of the downcomer. At the top of the riser, the air-particle mixture entered the disengagement section described above. It was expected that the majority of the particles in the flow would be separated by the impact disk in the disengagement section and would be reintroduced in the flow loop via the downcomer.

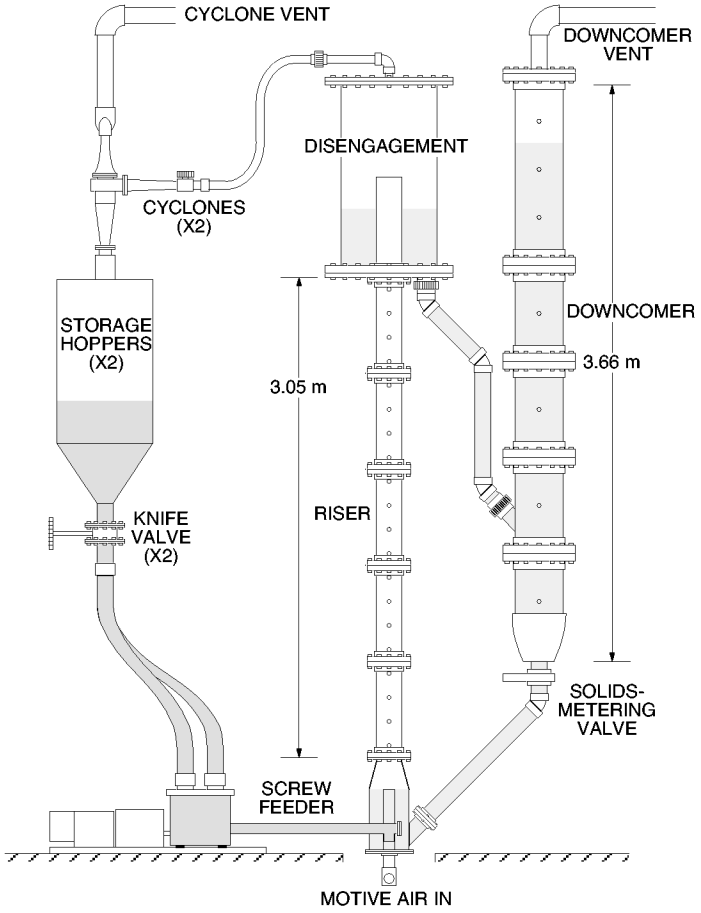

Figure 4 – Original Sandia riser configuration.

Air exited the disengagement section through 50-mm ID flexible tubing and flowed through two cyclone separators in parallel to remove any particles remaining in the stream. Separated particles dropped into a pair of storage hoppers and could be reintroduced to the motive air stream using a screw feeder. It was expected that the rate of particle collection in the storage hoppers would be relatively small and that this

secondary, batch-return process would be used only occasionally in riser operation. The air stream was exhausted from the building via a fan-driven, HEPA-filtered dust collector ("bag house"). Fluidization air was supplied at the bases of the downcomer, engagement, and disengagement sections, and along the solids transfer standpipes.

Construction of the riser facility in the ESEF was begun in the fall of 1998 and was performed by Sandia and contract technologists. Construction of the original configuration was completed in early summer of 1999, and the system was loaded for the first time with equilibrium FCC catalyst supplied by Chevron Research & Technology Company, an MFDRC member, in July of that year.

This original configuration demonstrated a pronounced unsteadiness in its solids loading and transport. This can be seen in the typical pressure time histories presented in Figure 5. Figure 5(a) shows the differential pressure signal across a section of the riser from $z_r/D_r = 16$ to $z_r/D_r = 18.2$ (here, $z_r = 0$ is defined as the junction plane between the engagement section and the first modular riser section). If particle acceleration is negligible (an assumption possible in the upper portion of the riser as well as in the downcomer), the differential pressure is proportional to the degree of solids loading in the measurement section. That is, the pressure drop across a section is the hydrostatic pressure required to support the weight of the particles in that section:

$$\Delta p = \rho_p \cdot g \cdot \Delta h \cdot (1-\varepsilon) \tag{1}$$

where Δp is the differential pressure across the measurement interval, ρ_p is the particle density, g is local gravitational acceleration, Δh is the vertical extent of the measurement, and ε is the mean void fraction (or gas volume fraction) in the measurement span. This interpretation of the differential pressure is included in Figure 5(a) as a second ordinate axis indicating the mean void fraction. In Figure 5(a), large spikes in pressure, corresponding to increases in solids loading, are apparent over periods of several minutes. The companion plot, Figure 5(b), shows the differential pressure in a section of the downcomer during the same run. The pressure in this trace was measured across the free surface of the bed in the downcomer and thus tracks the variation in bed height within the downcomer; this interpretation is included in Figure 5(b). At the beginning of the run, the downcomer is full of catalyst, so the surface of the bed is above the section across which the pressure is being measured. When the solids-metering valve is opened ($t \approx 200$ s), the bed level drops into the measurement section and is seen to oscillate on the same time scale as the loading in the riser. The solids valve is then partially closed for 400 seconds mid-run, reopened at about 1700 seconds, and is finally completely closed again at the end of the run; during both closures, the measurement section refills with catalyst. Note that when the solids valve is partially closed, the large spikes in loading seen in the riser (Figure 5(a)) vanish, suggesting that unsteadiness seen in the riser is related to large solids feed rates.

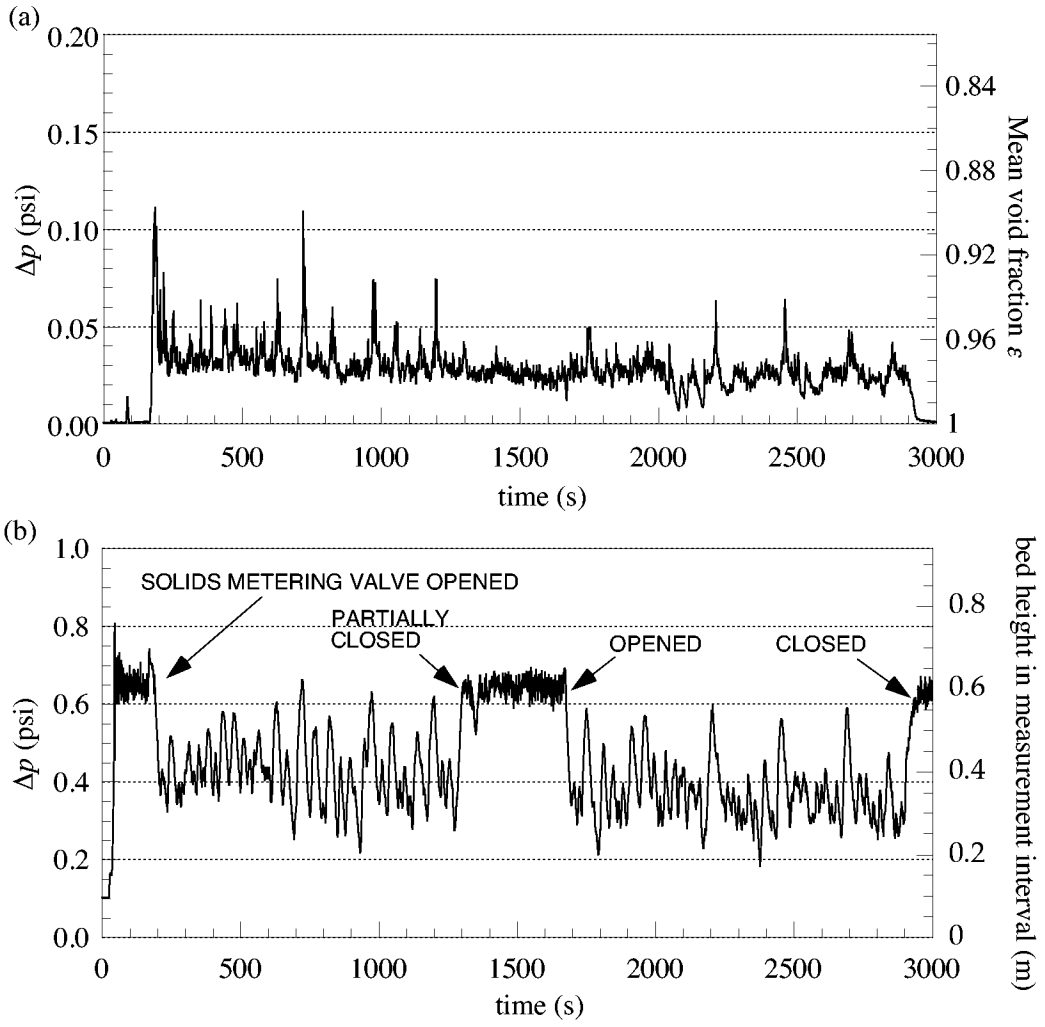

Figure 5 – Differential pressure traces in (a) the riser, and (b) the downcomer. The downcomer pressure trace reflects the behavior of the surface of the bed within the measurement section.

It was found that the nature of solids transfer from the disengagement section to the downcomer was oscillating between two conditions. In the first, solids flow in the standpipe connecting the two sections would choke, and solids would build up in the disengagement while the downcomer continued to empty into the riser. When the bed level in the downcomer would drop below some critical level, gas would bypass the disengagement section through the standpipe into the downcomer and exit the system through the downcomer vent instead of out the top of the disengagement and through the cyclones. This would aerate the standpipe sufficiently to release the particles in it, and the disengagement would empty back into the downcomer. As is apparent from Figure 5(b), this phenomenon occurred on a period of roughly 100-150 seconds.

Gas bypassing was also a problem in the system's other standpipe, transferring solids from the downcomer to the engagement section. Aeration gas from the standpipe and from the engagement section itself would travel up the standpipe and through the solids-metering valve into the downcomer. This presented a restriction to the solids moving downward through the valve and hence reduced the overall mass flux. The solids flow in the standpipe was generally unsteady and dilute, typically filling only about one-third to one-half of the standpipe's cross-sectional area.

Use of the screw feeder for secondary solids return also proved to be problematic. If the feed path was not sufficiently loaded with solids, a significant fraction of the motive air would bypass the riser and exit the flow loop via the screw feeder, hopper and cyclone in this secondary solids return leg. Additionally, the screw feeder outlet into the riser loop would at times pack with particles and impede any reintroduction of solids; the feeder, however, would continue to turn, further packing the particles that were already present. Eventually, the screw feeder was broken by this resistance, exacerbated by humidification problems that had allowed liquid water droplets to enter the riser base (Provisions for humidification of motive air for static-charge reduction were included in the riser design, and are discussed more fully in §6).

4. Modified Riser Configuration

The problems experienced with the initial riser configuration were mitigated by a series of incremental changes to the design. The final version of this modified riser is shown in Figure 6; this configuration reflects the accumulation of this series of step changes. Most noticeable is the elimination of the secondary particle return leg with its troublesome screw feeder and batch particle return. To accommodate this change, the cyclone separators were moved to the top of the downcomer, in turn requiring the shortening of the downcomer by 61 cm. Eliminating the batch return also resulted in a riser configuration that is more typical of the loops seen in industry, typified by the generic loop shown in Figure 1. The most striking difference between the laboratory riser and typical industrial units is the unique disengagement section, in which the majority of gas-particle separation is still achieved. Additionally, the cyclones in the Sandia riser are not fixed in a series arrangement, as in Figure 1; rather, the cyclones may be configured in series or in parallel. This allows a wider range of riser gas velocities with less effect on cyclone efficiency than would be seen in a fixed configuration.

To increase attainable mass flux in the riser by increasing the "solids head" in the downcomer during operation, the solids return point from the disengagement section to the downcomer was raised as high as possible. Raising the solids reintroduction point resulted in the construction of a horizontal solids transfer leg from the disengagement section to the downcomer. For larger particles (Geldart (1973) "Group B" particles), this 90° turn would constitute a non-mechanical valve, impeding the solids flow; however, for

particles of FCC catalyst's size and density range (Geldart "Group A"), this arrangement is acceptable if sufficient aeration is provided. Constructing an "L"-shaped down-turning extension of this standpipe inside the downcomer was found to restrict gas bypassing from the disengagement section to the downcomer. This bypassing was also restricted by reducing the size of the downcomer exhaust pipe.

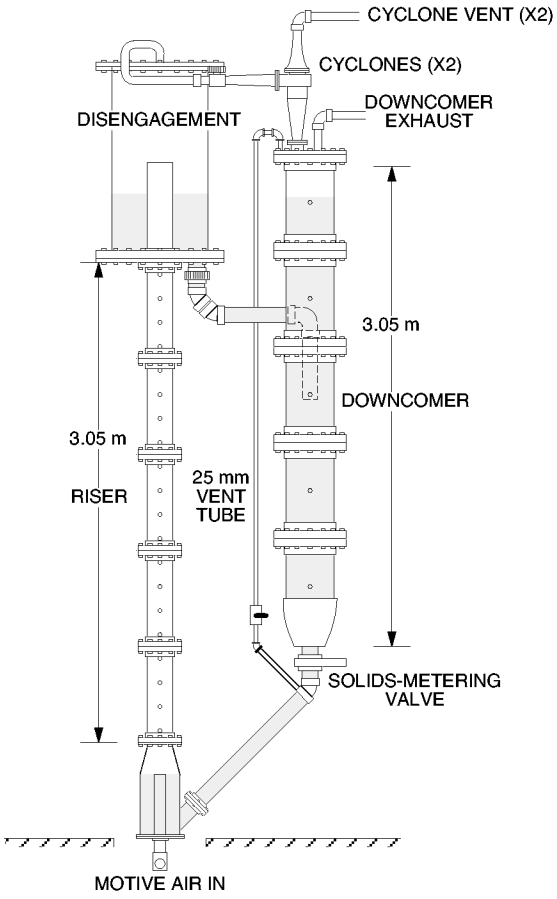

Figure 6 –Sandia riser after flow-loop modifications.

To overcome intermittent choking of the solids valve at the downcomer base by gas flowing up the standpipe into the downcomer, a 25-mm ID vent line was added connecting the top of the standpipe to the relatively low-pressure region at the top of the downcomer. This solution was explored by Karri *et al.* (1995), who found that it significantly raised the solids throughput of an angled standpipe. In the present installation, the vent line loads with solids and then effectively behaves as a fluidized bed through which large slugs of gas flow to the top of the downcomer. Steadiness of solids flow through the downcomer-to-engagement standpipe was observed to improve considerably with the installation of this vent.

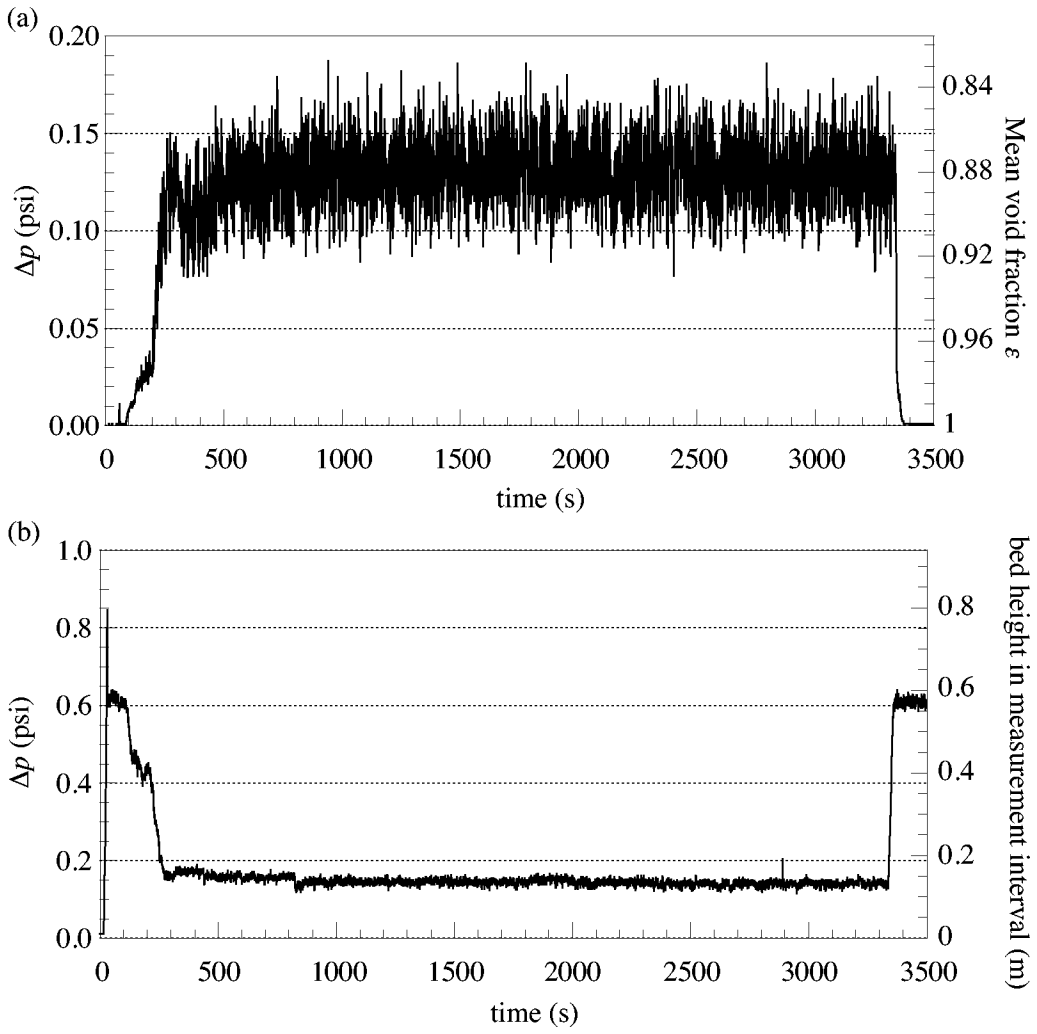

Figure 7 – Differential pressure traces in (a) the riser and (b) the downcomer for the configuration shown in Figure 6. The downcomer pressure trace reflects the behavior of the surface of the bed within the measurement section.

The combined effect of these modifications is shown by examining the pressure traces presented in Figure 7 for the modified riser configuration and comparing them to the original-configuration data shown in Figure 5; data in each figure are for the same positions in the two flow loops, and, as in Figure 5, interpretations as void fraction and bed height are included. Figure 7(a) shows differential pressure in the section of the riser from z_r/D_r = 16.0 to 18.2, while the pressure trace following the downcomer bed level is shown in Figure 7(b). From both figures, it is apparent that steadiness of operation has been increased dramatically, and Figure 7(a) indicates that solids loading (solids volume fraction) in the riser has been increased as well. While the magnitude of fluctuation in

Figure 7(a) is considerably larger than that in Figure 5(a), this behavior is consistent with the increased solids loading that has been achieved; the fluctuations are not related to overall system unsteadiness as in Figure 5. The pressure following the downcomer bed level shown in Figure 7(b) reflects the operational steadiness that has been achieved in the riser flow loop.

5. Extended Riser Configuration

One consistent criticism of the Sandia riser configuration described above is that it has a very low aspect ratio (height/diameter) relative to industrial facilities. It was recognized that this shortcoming was likely to limit the use of the Sandia results by MFDRC partners, and that it posed a barrier to comparison of Sandia riser data with previously published work. To address this, a 211 cm extension of the riser was designed that would increase the aspect ratio of the riser from its initial value of 25 to a value of about 40.

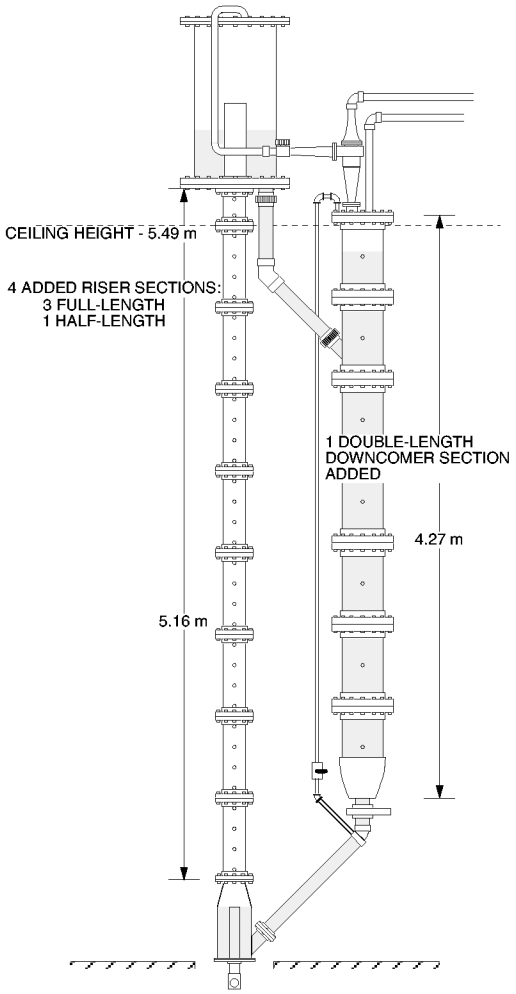

Figure 8 – Sandia riser configuration after extension through Building 865 roofline.

This extended configuration, shown in Figure 8, required the construction of an enclosed opening in the Building 865 roof and extension of the riser framework. Construction of this extension was begun in late June, 2000 and completed in September. Initial operation has begun; results will be presented in subsequent reports. *Data presented in this report were collected in the modified "short" riser configuration described in §4.*

6. Triboelectric Effects

Solids flow through the predominantly acrylic riser facility resulted in the generation of high levels of triboelectric charge (static electricity resulting from repeated catalyst-surface contact). This resulted in the static attraction and attachment of a thin layer of FCC catalyst to essentially all interior surfaces of the riser and occasional audible and visible electrical arcing to ground outside the riser. The former condition degrades experimental performance, limiting visual access to the riser flow; the latter presents a hazard to personnel and to diagnostic electronics.

To mitigate these effects, an extensive grounding system was included in the original riser design. This comprises braided steel grounding bands connected to an external ground bus, which is in turn connected to the building ground. The grounding includes the riser loop's components, the flow supply and exhaust systems, and the riser support structure itself. The riser installation also incorporates grounding rods that are used to ensure that a particular section of the riser is grounded before work is performed on that section. A humidification system was also installed in the riser air supply leg. Humidity is believed to increase the particles' surface conductivity, allowing more effective dissipation of surface charge, and has been used for static charge control in other cold-flow riser units (Deng, 1997). The air supplied to the riser from the wind tunnel compressor system is dried to humidity levels below 1%.

Initial tests with the humidification system produced mixed results. An increase in inlet air humidity was indicated by a humidity meter installed in the flow loop, and particle cling on the riser walls diminished considerably. However, operating the humidification system for periods longer than five or ten minutes resulted in the collection of liquid water at low points in the air supply system. Apparently, not all the water supplied for humidification was evaporating, or else the injected water was evaporating but later condensing out of the air. Worse, it appeared that this liquid water was mixing with catalyst, causing particle clumping in portions of the riser. It is believed that this may have been a contributing factor in the failure of the screw feeder, as the moisture exacerbated the solids packing problem described above. Evidence that there had been standing water at the screw feeder's outlet into the air supply line was found when the system was disassembled.

Examination of the humidification system suggested that some of the liquid water collection in the riser plumbing was not the result of condensation but of overspray. The original humidification system used a 70° spray cone, and was installed in a tee in the main air inlet plumbing. This wide cone angle resulted in spray impacting the pipe walls and never evaporating at all, instead producing a shear-driven liquid film that eventually collected at low points in the system. Replacement of the 70° nozzle with a narrower, 20° unit resulted in significantly less liquid collection in the riser plumbing. The original and modified humidification nozzle arrangements are shown schematically in Figure 9.

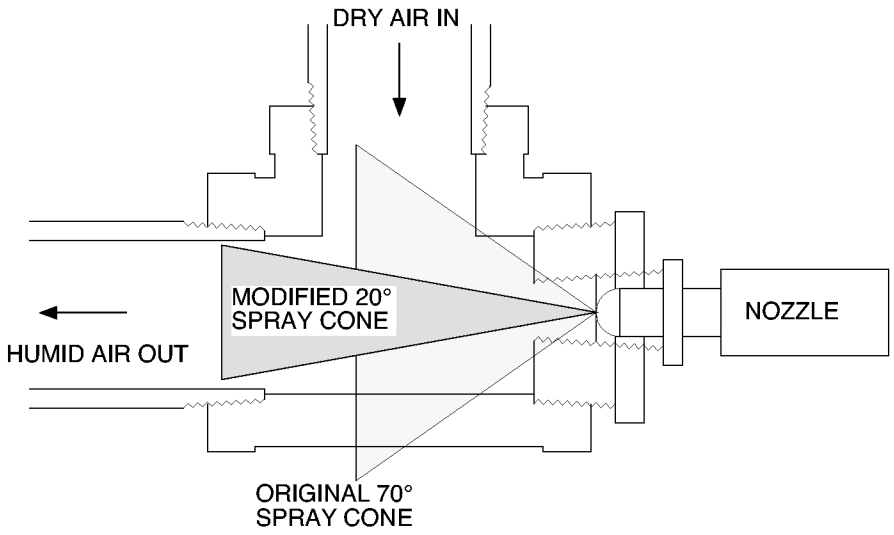

Figure 9 – Detail of humidification system as installed in air supply line, showing original and modified spray cone angles.

Further analysis revealed that the humidity levels of 60-80% initially sought in the riser were unattainable. An energy balance shows that the latent heat removal required to evaporate the amount of water required by such humidity levels at the supplied air's input temperature would result in a drop in air temperature to levels below lower saturation temperatures. In other words, the water required to achieve the humidity levels sought at the supply temperature would result in levels over 100% after evaporative cooling was considered. While this could be overcome by pre-heating the inlet air, it was decided to instead investigate the riser's behavior with whatever humidification was achievable.

A trial-and-error approach was taken to address the issue of maximum humidity practically attainable with the new nozzle configuration, and it was found that the riser could be run at humidity levels of 10-15% without experiencing liquid collection. These relatively low humidity levels were still sufficient to produce significant benefits in terms

of both visual access and static discharge. However, it was found that after several cumulative hours of running at this level of humidification, the behavior of the particle inventory in the riser began to change. With no other changes to riser configuration, more particle bridging and intermittent ("slip-stick") flow were observed. It was surmised that the zeolite base of the FCC catalyst used in the riser was absorbing moisture and changing the powder's properties, particularly its cohesiveness. The powder was dried by fluidizing with dry air for several days, after which it reverted to its previous behavior. Deng (1997) did not note any such problems; however, he used sand as particles in his system, which would presumably be less hydrophilic than the zeolite-based FCC catalyst. Industrial MFDRC partners, meanwhile, have suggested that the increased cohesiveness seen in the FCC catalyst due to humidification can be overcome by increasing aeration rates in the flow loop. A systematic study of this solution has not yet been made.

Static charge can also be reduced using a commercial antistatic additive; one example is the Larostat™ family of quaternary ammonium compounds produced by BASF (BASF is not an MFDRC member company). However, use of these additives – even in the small quantities recommended by their manufacturers – poses several problems. One is that the addition of an antistatic agent will have an effect on particle properties. While effects on such quantities as density or size distribution would likely be small, effects on second-order quantities such as interparticle cohesion could be significant while also being difficult to characterize and account for in measurements and computational models. The addition of an antistatic additive would also impose additional logistical details addressing health and safety concerns; these issues have yet to be fully explored. Finally, such additives are most effective when some humidification is added to the flow as well, which reintroduces the concerns discussed above.

In summary, it appears that, while the use of humidification is a viable solution for short-term static control, its continued long-term use, even at low levels, is complicated – but not precluded – by the absorption of moisture by the zeolite-based FCC catalyst powder. It may be possible to address these complications by adjusting fluidization air supply rates in the riser; this will be examined in future experiments.

7. Mass Flux Diagnostics Development

In addition to the pressure and flow diagnostics described above, work has progressed on the development of means for the measurement of solids flux in the riser. Efforts were made to measure mass flux by timing a visually observed particle's drop along the downcomer, a technique used in the past by several workers (*e.g.*, Miller and Gidaspow, 1992; Zhou *et al.*, 1994). The high degree of uncertainty in applying this method in the Sandia riser was realized when it was observed that a measurement made with the slide valve completely closed (*i.e.*, a case in which the solids flux is definitely zero) would still result in a mass flux estimate of 16 $kg/m^2 \cdot s$. It was surmised that this was an artifact of particle recirculation induced by the fluidization air flow in the

downcomer. Two other techniques for mass flux measurement have been investigated: porous valves for global (bulk) mass flux measurement, and mass flux probes for local measurements.

7.1 Mass Flux Measurement by Porous Valves

The idea of using a porous valve for riser mass flux measurements has been applied by several workers in the past (see, *e.g.*, Issangya *et al.*, 1998). In this technique, a porous valve is included somewhere in the non-riser portion of the flow loop. The porosity is selected to encourage bridging of particles while still allowing the flow of gas past the valve. When the flow of interest in the riser is established, the valve is quickly closed, and the rate at which solids inventory below the valve drops (or solids build up above the valve) is measured. From this rate, the bulk particle density at the measurement location, and the cross-sectional area of the measurement location, the mass flux in the riser can be calculated as:

$$G_s = -\rho_s \cdot \frac{dh}{dt} \cdot \frac{A_{c,measurement}}{A_{c,riser}} \tag{2}$$

Because the pressure in a stationary or slowly-moving fluidized bed is dominated by the hydrostatic pressure due to the particles themselves, it is often more practical to infer bed height from the bed pressure (eq. 1; note that the bulk density ρ_s in the downcomer is the particle density ρ_p scaled by the downcomer-bed solids fraction $(1-\varepsilon)$). The relationship between riser mass flux and the pressure in the downcomer bed can be manipulated to obtain:

$$G_s = -\frac{1}{g} \cdot \frac{dp}{dt} \cdot \frac{D^2_{downcomer}}{D^2_{riser}} \tag{3}$$

The implicit assumption in applying this technique is that the valve's porosity minimizes its impact on the flow loop during a relatively short-duration measurement. The validity of this assumption can be examined by comparing the riser's pressure profile during the measurement to the profile before and after the measurement.

A porous valve was fabricated for the Sandia riser by perforating the valve plate in a standard knife valve. The holes are 1.59 mm in diameter, and are spaced on a 3.18-mm pitch in a square pattern, for a porosity (open area per unit area) of about 20%. It was installed in the disengagement-to-downcomer standpipe as indicated in Figure 10. The valve is manually actuated by a short-throw lever; relative to the time scales of the measurement, the time required to open the valve is believed to be small enough for its associated transient to be neglected.

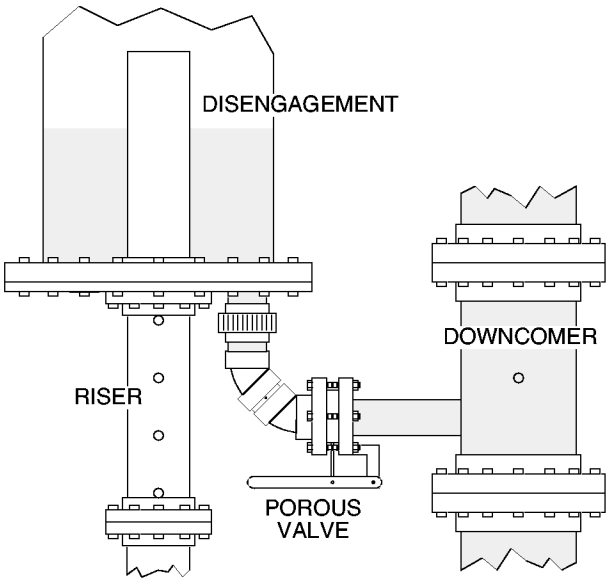

Figure 10 – Detail of disengagement-to-downcomer standpipe showing location of porous valve installation for mass-flux measurement.

A time history of the differential pressure across a section of the downcomer for a set of porous-valve measurements is shown in Figure 11(a). As in Figure 5, the section of the downcomer for which the measurements are presented was selected to include the free surface of the particle bed in the downcomer, and changes in the differential pressure across the section mimic the changes in the height of the bed. This time history includes porous-valve closures of 10- and 20-second durations for solids-metering slide-valve positions of 100%, 50% and 20% open area. At each porous valve closure point, it is possible to fit a straight line to the downcomer differential pressure trace, the slope of which gives the dp/dt term in Equation 2. This is demonstrated in Figure 11(b).

Figure 11(a) also demonstrates some interesting characteristics of the riser flow unrelated to the porous-valve mass-flux measurement. The effect of the solids-metering valve is clearly non-linear: little difference in downcomer inventory results from the change in solids-metering valve position from 100% to 50% open area, but the change effected by reduction from 50% to 20% is considerable. The apparent quick return of the downcomer bed level to its initial height at the end of the run is somewhat deceptive. The pressure trace presented only spans a segment of the downcomer selected to include the bed's free surface during the riser run; when the metering valve is closed, the free surface is outside the spatial interval over which Δp is measured. The downcomer's return to its pre-run level is more asymptotic in nature. Figure 11(a) only presents the early phase of this behavior, *ca.* 1800 s.

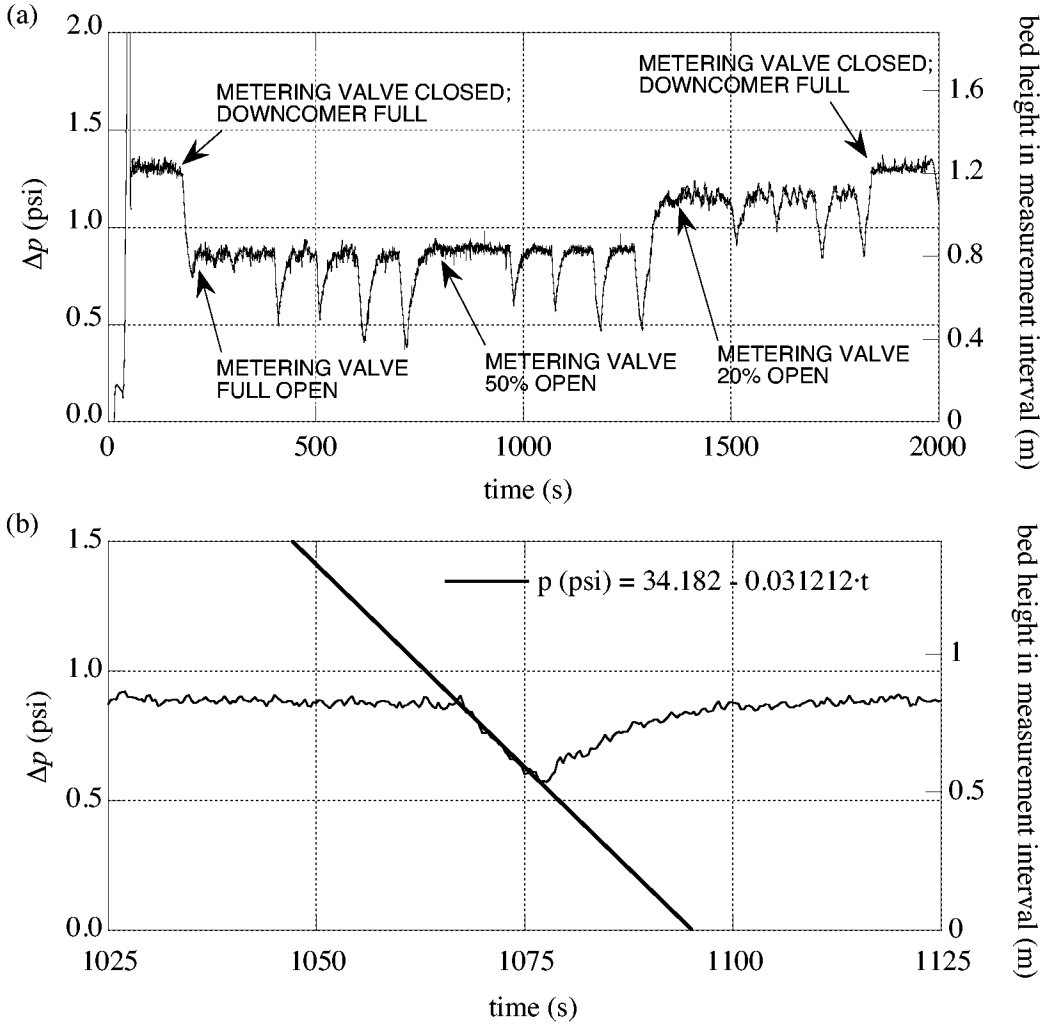

Figure 11 – Differential pressure trace in downcomer indicating height of bed surface during porous-valve closures for mass flux determination: (a) complete time history in which each negative Δp spike corresponds to a porous-valve closure; (b) trace for a single porous-valve closure, showing application of linear curve fit to determine mass flux from rate of bed-height decrease.

Figure 12 shows the downcomer differential pressure traces from Figure 11 that correspond to the porous-valve closures for the solids-metering valve position of 50% open area; each trace has been offset such that $t = 0$ is the time of porous-valve closure. While consistent behavior is demonstrated among the four traces, it is also visually evident in the 20-second-closure traces that the differential pressure (and, by extension, the downcomer bed height) is not dropping linearly. This is physically reasonable: as the bed height drops, the pressure pushing solids through the metering valve drops

accordingly, lowering the actual flux. This suggests that the later portion of the pressure trace should be discarded in performing a linear curve fit. Alternatively, a more general fit could be adopted (*e.g.*, a quadratic profile) and its slope evaluated at the instant of valve closure.

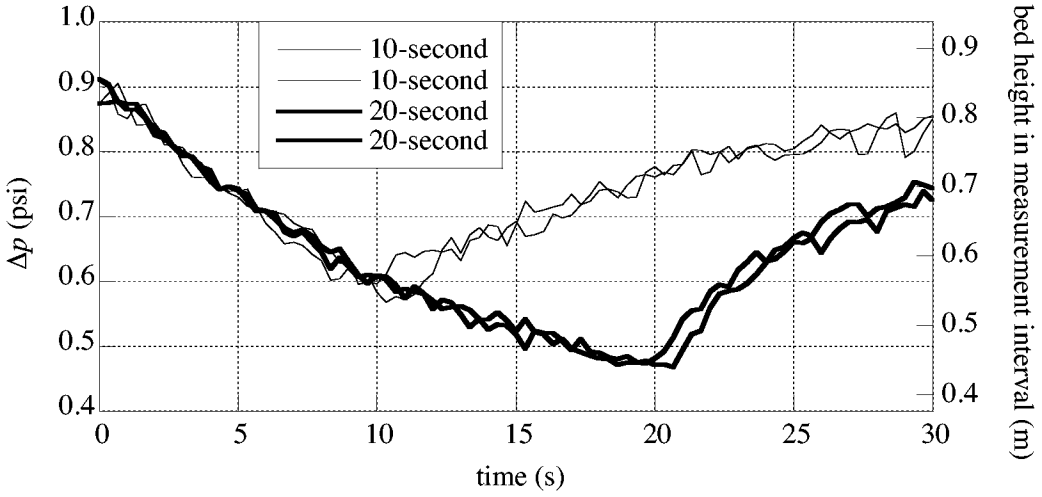

Figure 12 – Differential pressure traces in downcomer indicating height of bed surface during porous-valve closures in 50%-solids-metering case.

To further investigate the effect on the estimated mass flux of this non-linearity, linear fits to the differential pressure data were performed with the lower bound of the fit domain at $t = 0$ (the valve closure time), but varying the upper bound of the fit. Figure 13 shows the resulting mass flux estimates for the traces shown in Figure 12; the trends displayed are typical of all cases examined. For fit domains larger than five seconds, the estimated mass fluxes drop nearly monotonically in all cases. This is consistent with the behavior seen in Figure 12, in which the differential pressure curves flatten with increasing time. This would drive the linear fits' slopes to lower magnitudes and reduce the associated mass flux estimate. For fit domains under five seconds, the trends diverge. This is a reflection of the smaller sample size increasing the sensitivity of the regression to the scatter among individual points in the fit domain and suggests that results from fits in such small domains are unreliable. Examination of Figure 13 provides some indication of uncertainties in this measurement: for domains of five to ten seconds in duration, the uncertainty attributable to domain size and the uncertainty associated with the system's repeatability are each about ± 5 kg/m^2·s. The magnitude of these variations remained relatively constant with solids-metering valve position. The effect of data scatter on the measurement could also be mitigated by increasing the data sampling rate significantly (*e.g.*, to 100 Hz.) during the valve closure.

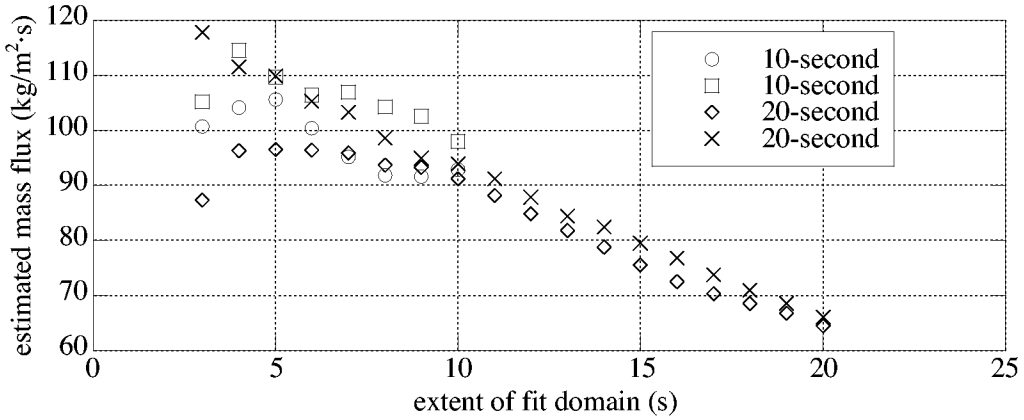

Figure 13 – Effect of fit domain on estimates of mass flux from differential pressure traces in Figure 11.

The effect of the porous valve closure on the riser flow can be seen by examining the differential pressures in sections of the riser. Three of these are presented in Figure 14 at low, middle and high positions in the riser. In each plot, time histories of differential pressures across a 305-mm length are plotted for the four porous-valve closures in the 50% solids-metering case. A line representing the time mean of the differential pressure at the same location and conditions but with the porous valve open is included in each figure for comparison. For each trace, the time $t = 0$ corresponds to the porous-valve closure time. Figure 14(a) shows the differential pressure in the span $0.8 \leq z_r/D_r \leq 2.9$ (again, $z_r = 0$ is the junction of the engagement section with the first modular riser section). The measured differential pressure in this section increases when the porous valve is closed; in the two 10-second-closure cases, the return to near-mean conditions takes about as much time as the rise. Figure 14(b) shows the pressure drop in the section $7.3 \leq z_r/D_r \leq 9.5$; this trace, typical of its neighbors, shows no discernable pattern of deviation about the mean signal, such that differential pressure in the middle portions of the riser are relatively unaffected by the porous valve's closure. Figure 14(c) shows the pressure drop in the section $18.2 \leq z_r/D_r \leq 20.4$ (while this is the uppermost differential pressure measurement station on the riser, it should be borne in mind that the riser extends another 45 cm into the disengagement section). At this location, the differential pressure drops when the porous valve is closed. However, in both the 10- and 20-second-closure cases, it continues to drop for about seven seconds after the valve is re-opened, after which it returns to levels near its mean. The cause of this continuing drop is unclear.

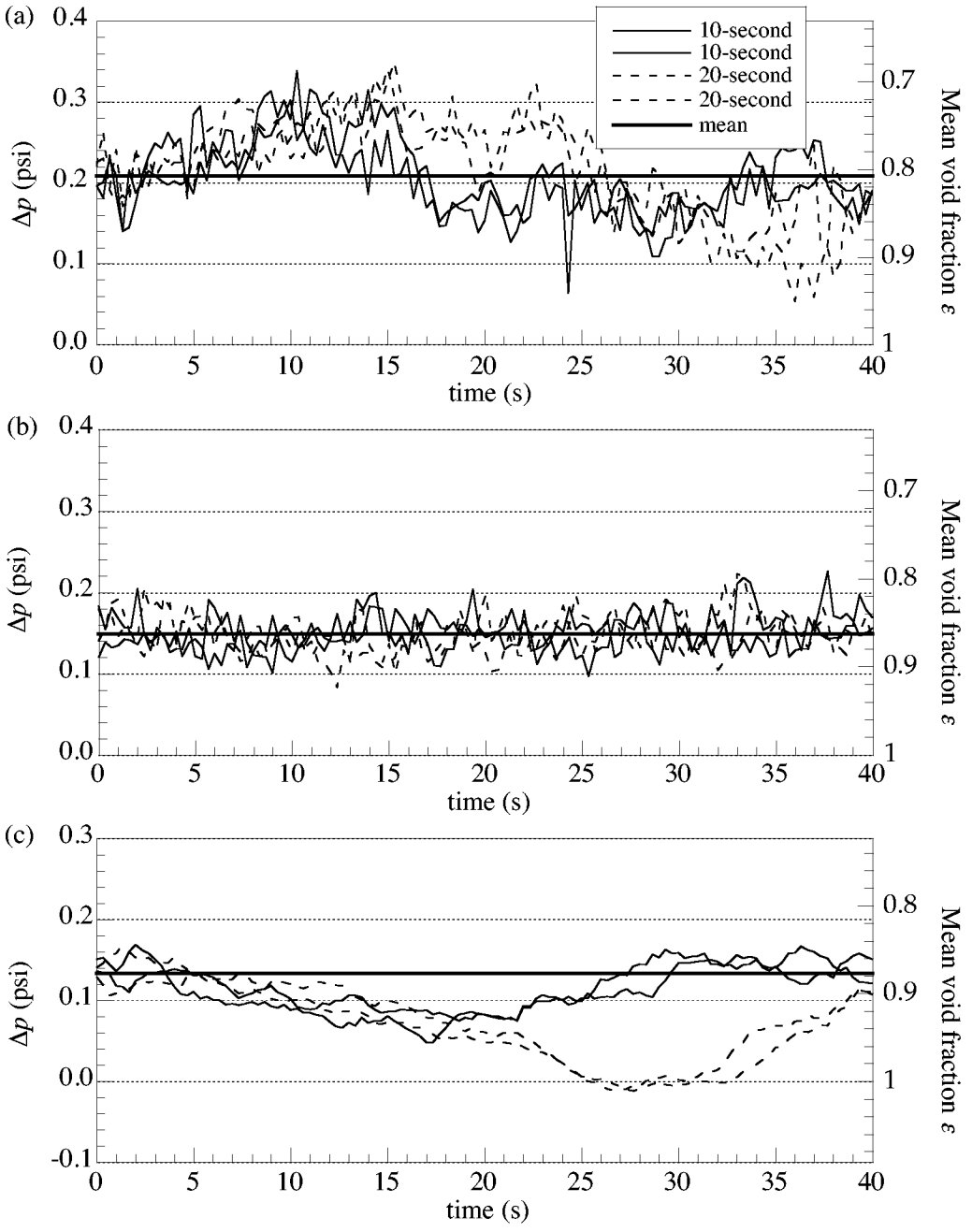

Figure 14 – Differential pressure traces in riser sections during 10- and 20-second porous-valve closures for 50%-solids-metering case. Traces are offset so that time $t = 0$ corresponds to the valve closure time. Pressures measured across sections spanning (a) $0.8 \le z_r/D_r \le 2.9$ (b) $7.3 \le z_r/D_r \le 9.5$, and (c) $18.2 \le z_r/D_r \le 20.4$. "Mean" line indicates time-mean of Δp with porous valve open.

In summary, examination of a porous valve for mass-flux measurement has demonstrated that use of such a valve affects the flow in the riser, particularly near its base and disengagement sections. Any porous-valve measurement results should be viewed in this light. The sensitivity of the measurement to the analysis domain must also be considered carefully, as demonstrated in Figures 12 and 13. However, the relatively small deviations about the mean seen in the early portions of the traces in Figure 14 suggest the possibility that the effects of porous valve closure on riser flow are not significant in the first five seconds of closure – at least when differential pressure is used as a metric of effects – and so the porous valve measurement might be considered most reliable when analyzed over this domain. On this basis, and with the above discussion taken as a qualification, the porous-valve data suggest that the maximum mass flux achieved in the riser for the operating condition studied is approximately 110 $kg/m^2 \cdot s$, with a precision uncertainty of order ± 10 $kg/m^2 \cdot s$.

7.2 Mass Flux Measurement by Suction Probes

Several workers have made measurements of mass flux in risers using suction probes. In this technique, a sampling tube is inserted parallel to the riser mean flow, and a sample of gas and solids is withdrawn from the column. The mass flux normal to the probe can then be determined from the resulting sample mass, sample time, and the sampling area presented normal to the flow. The net mass flux in any particular direction can be determined from the difference in opposing fluxes measured along that direction. An important proviso in this technique is that the sample is isokinetic, *i.e.*, the gas velocity of the suction must match the local riser gas velocity in the sampling direction. A low suction velocity results in an underestimation of mass flux, while a high suction velocity results in an oversampling of particles. In addition, failure to achieve isokinetic conditions can result in a sampled particle size distribution that is not representative of the local size distribution in the riser. Isokinetic sampling in a variety of gas-solid flows has been attempted by several groups, including van Breugel *et al.* (1969), Nguyen *et al.* (1989), Harris and Davidson (1992), Coronella and Deng (1998), and Reinhardt *et al.* (1999).

The difficulties presented by isokinetic sampling include the inability to match the suction and riser gas velocities beyond a time-mean sense and the practical requirement that some suction always be applied to prevent probe plugging, even in cases where this is clearly physically unrealistic (consider an upward-facing, downward-sampling probe in an upward-flowing gas stream). Several workers (*e.g.*, Miller and Gidaspow, 1992; Rhodes and Laussmann, 1992; Zhang *et al.*, 1995) have overcome these obstacles using non-isokinetic sampling at suction rates far in excess of the local gas speed. While they found that increasing sample suction velocities spuriously increased values of directional mass fluxes, the net flux represented by their differences remained relatively unchanged and agreed well with independent estimates of mass flux.

The non-isokinetic suction sampling system used at Sandia is shown schematically in Figure 15. A vacuum pump is used as a suction source. The particle sample flows into a sample collector, in which a tangential entry imparts a swirling motion to the flow and separates the solids from the gas. The gas exits the sample collector through a shielded 10-micron filter and flows through a rotameter before being exhausted to atmosphere through the vacuum pump. To concentrate on development of the technique itself, refinements such as purge lines have been omitted from this system but will be included on the final system.

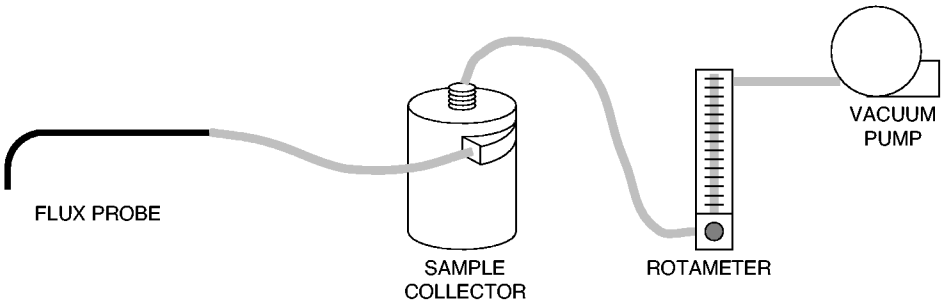

Figure 15 – Schematic diagram of Sandia flux probe system.

Two sampling probes were constructed. The first was 6.35-mm OD and 4.3-mm ID, with a 90° bend on a 14-mm center-line radius. Early tests with this probe quickly showed that it was prone to choking, in which the entire cross-section of the probe filled with catalyst moving in a plug flow. This choking is presumed to be a result of the probe's relatively small ID. A second, larger probe was also constructed, using 9.5-mm OD, 7.4-mm ID stainless steel tubing, with a 90° bend on a 24-mm center-line radius; this probe is shown in Figure 16. The 73-mm vertical sampling leg is relatively long to avoid effects of the horizontal leg's wake when sampling particles moving opposite to the mean gas flow. This larger-ID probe became the focus of development efforts.

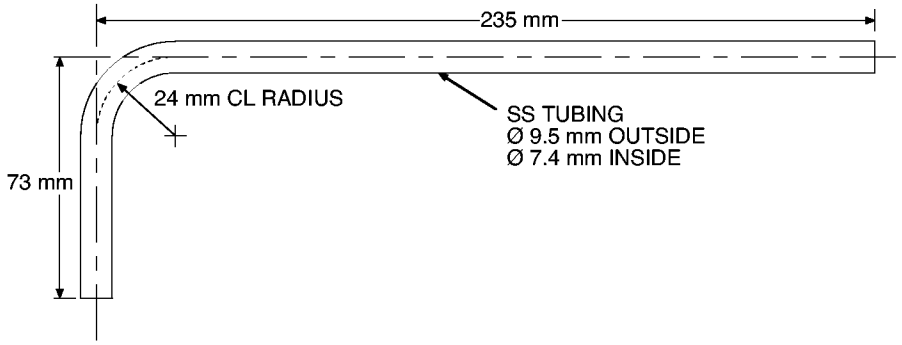

Figure 16 – Drawing of 9.5-mm OD, 7.4-mm ID flux probe.

Results for the 9.5-mm OD probe are shown in Figure 17. Each of these figures includes results for upbound and downbound flux measurements, and the net flux profile obtained from the difference of the two curves. Figure 17 shows two sets of measured flux profiles for the condition $U_g = 5$ m/s, with a "true" mass flux later estimated to be 110 kg/m^2·s using the porous valve technique described above. The probe is inserted at a height of 239 cm, or $z_r/D_r \approx 17$ (as before, $z_r = 0$ is defined as the junction plane between the engagement section and the first modular riser section). In both cases, the probe traverses the riser in the riser-standpipe-downcomer plane. The particle-sampling gas velocity is estimated to be about $1.7 \cdot U_g$. The profiles in Figure 17(a) are for the case in which the probe is inserted into the riser column from the side opposite from the solids entry to the engagement section from the downcomer (the solids-entry side is designated as positive r, *i.e.* $r/R_r = +1$ on this side); the profiles in Figure 17(b) are for probe insertion from the same side as particle entry. In each case, data are not available close to the "near" wall of the traverse (*i.e.*, the wall through which the probe is inserted) because the curvature of the probe precludes its withdrawal to the extent necessary to reach these points.

Some asymmetry is apparent in Figure 17(a), with the downbound and net flux profiles biased towards higher fluxes on the far side of the traverse. This side corresponds to the side on which particles are fed into the riser, and so this result, viewed alone, suggests that the entrainment of particles from the fluidized bed in the engagement section may not be axisymmetric but biased towards the feed side of the section. However, in Figure 17(b), in which the experimental conditions are repeated but the probe insertion is from the particle-feed side of the riser, the asymmetry reverses. This reversal contradicts the above inference that entrainment in the engagement is biased towards the particle-feed side. Rather, it suggests that the bias in the profile is an artifact of the measurement technique.

A possible source of this bias is probe-wall interference. As the probe's distance to the wall is decreased, it begins to present an obstacle to the down-flowing particles on the wall. This results in an artificially high concentration of particles near the probe tip, which are then sampled by the probe's suction. In the case of downbound particle sampling, shown schematically in Figure 18(a), the probe's sampling tip is close to the dense particle cluster that is formed. In the case of upbound particle sampling (Figure 18(b)), however, the tip is relatively removed from the falling particles clustered by the probe's presence, and so the resulting bias in the measurement is smaller than in the downbound-sampling case. It is also possible that falling particles are concentrated less effectively by the probe in its upbound-sampling orientation because the probe's radius presents less of an obstruction to these particles. It should be noted that this discussion is *not* an effort to explain large concentrations of particles near the wall; a dense, down-flowing annular region is an empirically well-established characteristic of CFB flows. Rather, this is an effort to explain the bias towards higher fluxes that is seen at the wall opposite probe insertion in the present data.

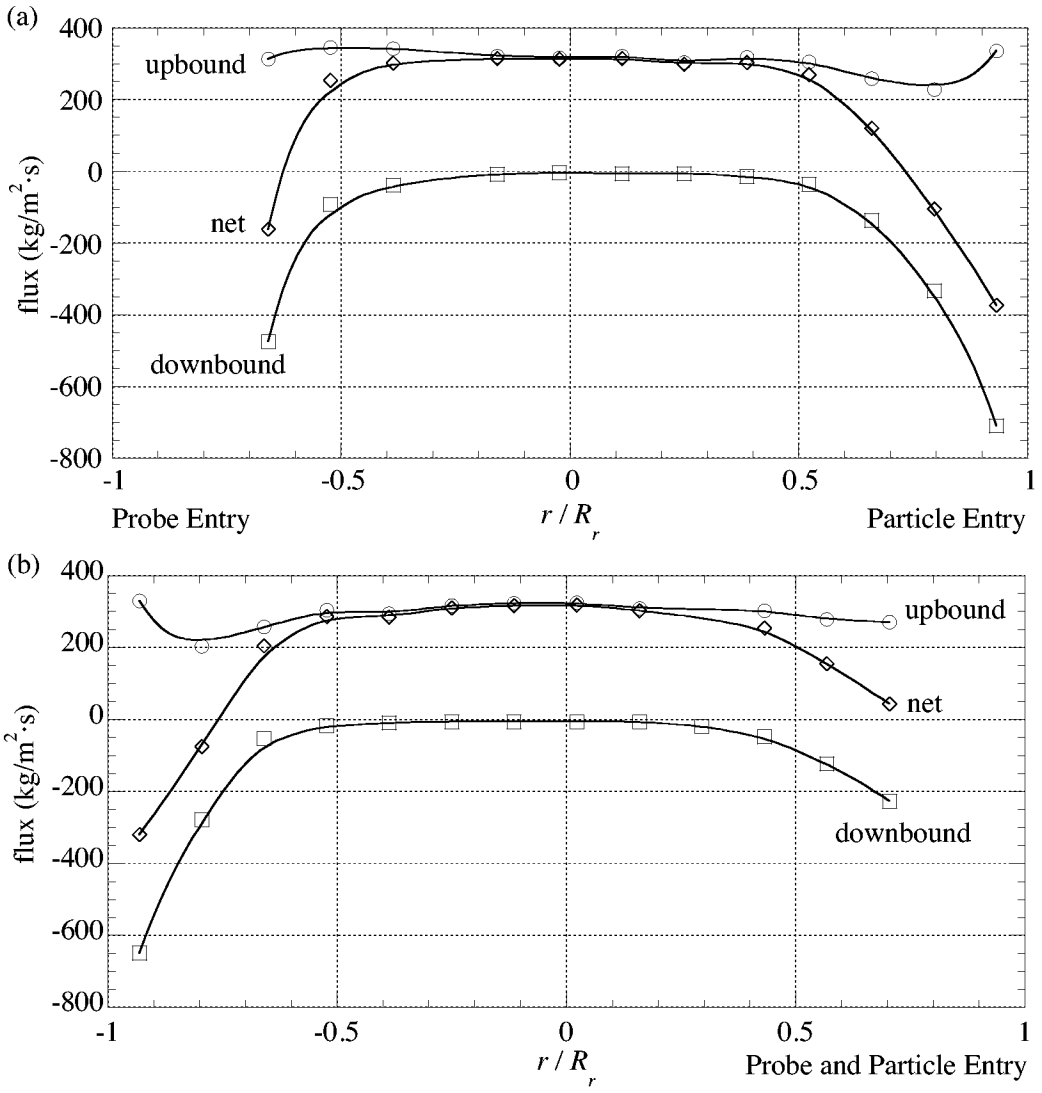

Figure 17 – Flux probe measurements in the riser at z_r/D_r = 17. (a) probe inserted from side of riser opposite particle entry to engagement section; (b) probe inserted from same side as particle entry.

Despite the relatively large diameter of the 9.5-mm probe, it is still prone to choking in high-particle-loading situations; this is probably due to insufficient suction provided by the vacuum pump used as a motive source. This introduces large uncertainties to each flux measurement, which become very significant when the individual values are differenced to estimate the net flux. The compounded effect of this systematic error source is seen when the net flux profile is integrated to obtain a bulk flux in the riser. For the high flux cases described above, integrating the "complete" side of

each profile (*i.e.*, assuming a symmetrical profile, and integrating the half of the profile that extends to the riser wall) gives flux estimates of 4.5 and 41 kg/m^2·s.

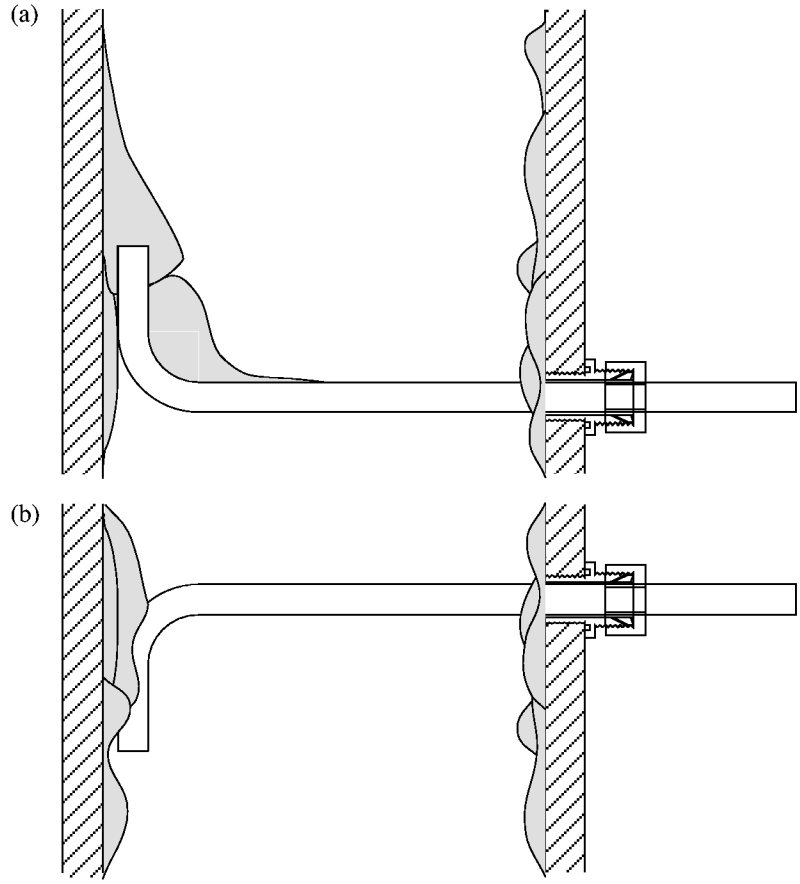

Figure 18 – Proposed explanation of bias mechanism in downbound near-wall flux probe samples. (a) particle concentration at probe tip in downbound sampling position. (b) probe self-shielding in upbound sampling position.

Figure 19 shows mass flux profiles for the case U_g = 5 m/s, with a mass flux estimated from porous valve measurements to be approximately 20 kg/m^2·s. As in Figure 17, profiles in this figure are in the riser-standpipe-downcomer plane. The probe is inserted from the same side of the riser as the solids entry to the engagement section. Again, an asymmetry in the measured profile is seen, but this asymmetry differs from that seen in the more densely loaded profiles of Figure 17 in two ways: the asymmetry now dominates the upbound, rather than the downbound, flux profile; and the profile shows larger mass fluxes on the particle-entry side of the traverse. Both of these differ from the

above discussion of possible causes of the bias seen in the densely loaded case. It is believed that the bias seen in the profiles in Figure 19 are a reflection of the riser's true behavior at these conditions, and suggest the existence of a bias in particle engagement for dilute operating conditions.

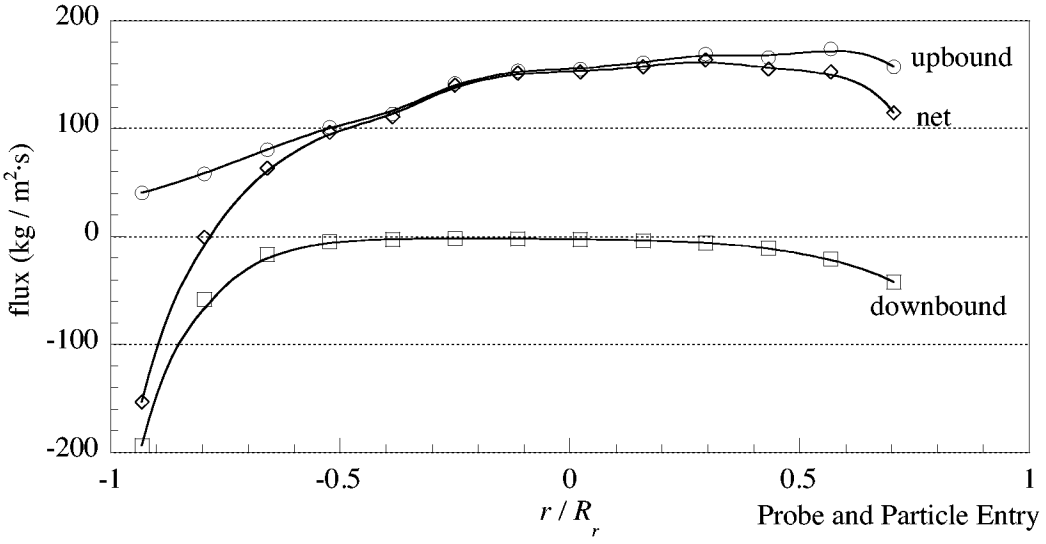

Figure 19 – Flux probe measurements in the riser at $z_r/D_r = 17$; probe inserted from same side as particle entry to engagement section.

As in the high-flux case, the uncertainties in the individual measurements are apparently comparable to the differences between the measurements that are used to estimate the net flux. For this low-flux case, integrating the "complete" side of each profile as in the high-flux case gives a flux estimate of 13 kg/m^2·s.

8. Particle Diagnostics

A complete description of gas-solid experimental results should include a description of the particles' shape, size distribution, and density. Each one of these factors has a direct effect on the hydrodynamics of the gas-solid flow.

Particle shape is most easily examined by microscopy, though rigorous characterization of either shape or size by this method is time-consuming. A microphotograph of fresh catalyst is shown in Figure 20. Particles are generally spherical, in the range of 30-100 microns in diameter, and are relatively smooth-surfaced in appearance. A few "double" particles, resembling intersecting spheres, are apparent in microscopic views. Used catalyst is shown in Figure 21; the catalyst sample shown in the image was collected from the bag house after about 10 cumulative hours of riser

operation. The particles in this sample have retained their spherical shape but have been coated with micron-scale, non-spherical fines.

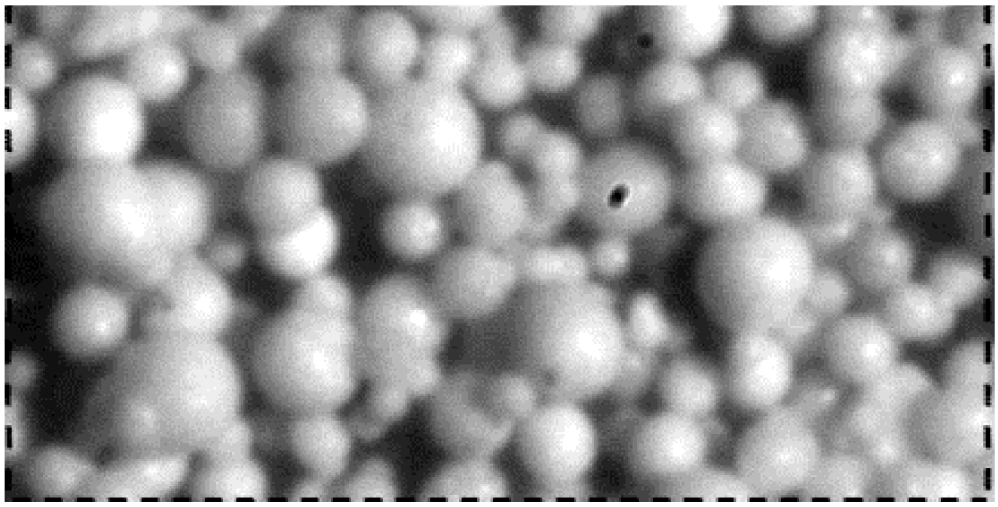

Figure 20 – Microphotograph of FCC catalyst before loading into the Sandia riser; photo dimensions are approximately 1000 microns horizontal × 500 microns vertical.

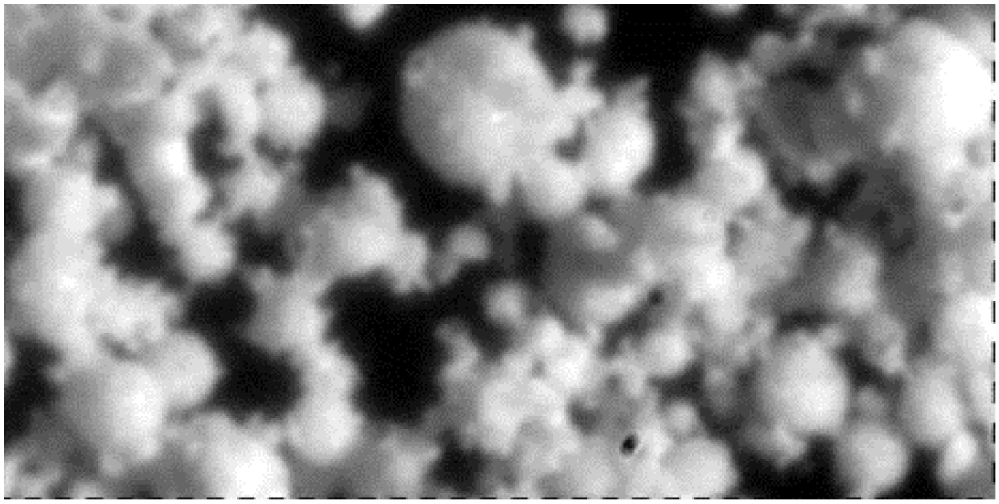

Figure 21 – Microphotograph of FCC catalyst collected from the Sandia riser bag house after nominally 10 hours of running; photo dimensions are approximately 1000 microns horizontal × 500 microns vertical.

Particle size distribution is analyzed using a Malvern 2600 laser diffraction apparatus. The basis of the measurement is a factory-calibrated analysis of the diffraction

of a laser beam passed through a suspension of particles. Reliable operation of the Malvern system, including proper sample preparation and presentation, has been verified by comparison to sieving and microscopy (individual particle counting) results. Particle size distribution results are shown in Figure 22 for fresh FCC catalyst and in Figure 23 for a sample collected from the bag house; note that these distributions are on a volumetric basis. Some segregation is apparent in the bag house sample, which displays a long fines tail in its distribution.

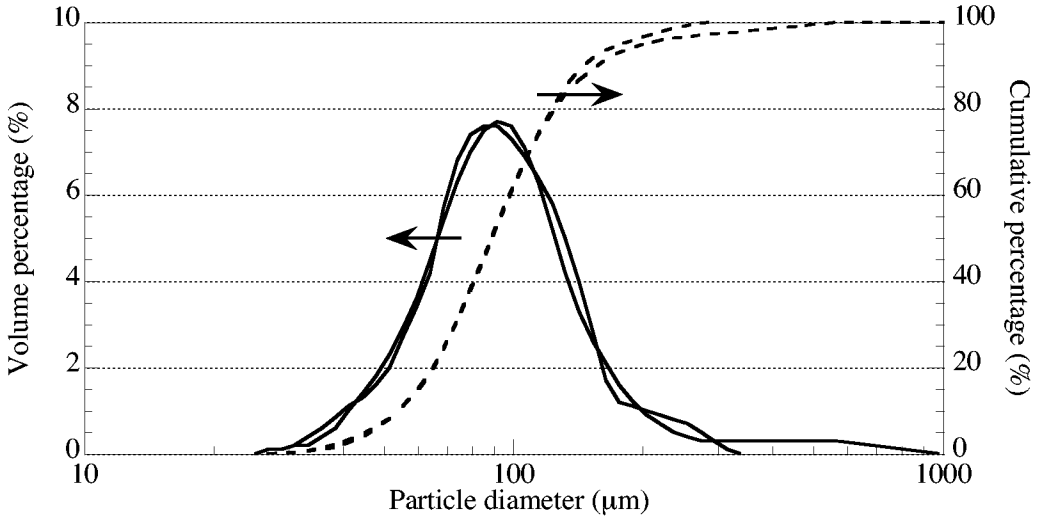

Figure 22 – Volumetric size distributions for two samples of fresh FCC catalyst used in the Sandia riser.

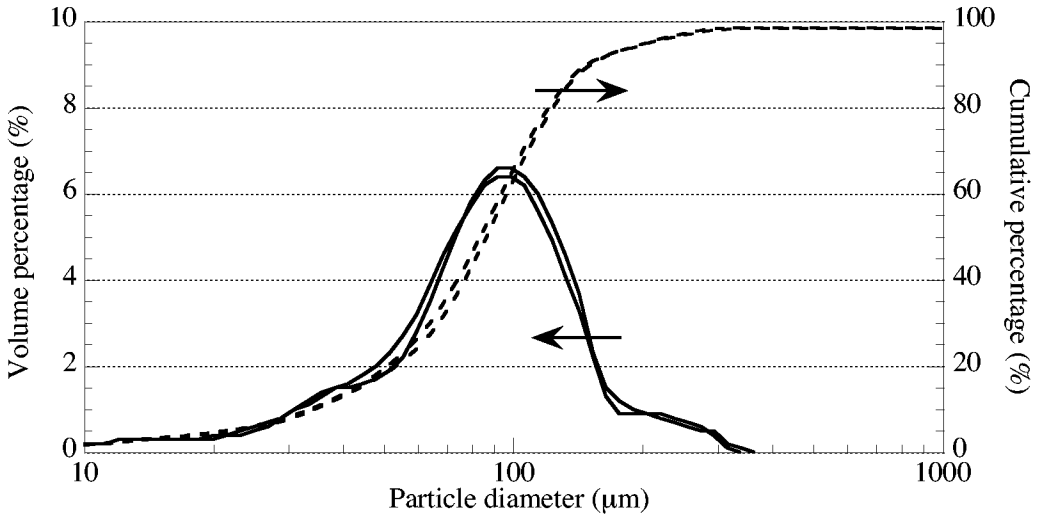

Figure 23 – Volumetric size distributions for two samples of FCC catalyst collected from the Sandia riser bag house.

9. Other Diagnostics and Future Work

In addition to continued development of the techniques described above, work is continuing to develop advanced non-intrusive diagnostics for application to riser flows. A three-dimensional particle image velocimetry (PIV) system has been developed, and preliminary measurements have been made of velocities of particles in a vertical plane in the riser. This optical technique is likely to be applied only to very lightly loaded flows.

A gamma-densitometry tomography (GDT) system is also in development for riser solids distribution measurements. GDT measurements have been performed previously at Sandia in a cold-flow bubble-column experiment (see, *e.g.*, Shollenberger *et al.*, 1997; Torczynski *et al.*, 1997). In these single-source, single-detector measurements, time-averaged gas-volume-fraction profiles were built up by traversing the source, its collimated beam, and a single detector in tandem across the column's diameter. For the MFDRC riser studies, multiple detectors will be used to receive a fan beam from a single source, which should allow the collection of quasi-instantaneous solids distribution profiles in a single cross-sectional plane of the riser. At the time of this writing, the source has been obtained, and traverse and mounting hardware have been designed and constructed. The gamma detectors are being evaluated individually for calibration and installation. A plan view of the Sandia riser GDT system is shown in Figure 24.

Fiber-optic probes for measurement of voidage and particle velocity are also targeted for use in the Sandia riser. In these measurements, light is transmitted into the riser through fibers in the probe; the reflected light is collected and transmitted through other fibers and is presumed proportional to particle concentration at the probe tip. Two types of fiber optic probes have been obtained. The first type, provided by MFDRC partner Dow Chemical, is described in Cocco *et al.* (1995). It uses single fibers for light transmission and collection. It is claimed that with careful calibration, probe data can be used to measure particle or particle-cluster velocities as well as concentrations. The second type is a multiple fiber probe purchased from Prof. John Grace's research group at the University of British Columbia. Similar probes are described in Zhou *et al.* (1994). Both types of probe depend on the development of an accurate calibration method. Initial results with both probe types have been mixed. While there have been successes, notably the detection of individual clusters and the generation of two-point cross-correlations of probe signals, there have also been difficulties with probe fouling and lack of calibration repeatability.

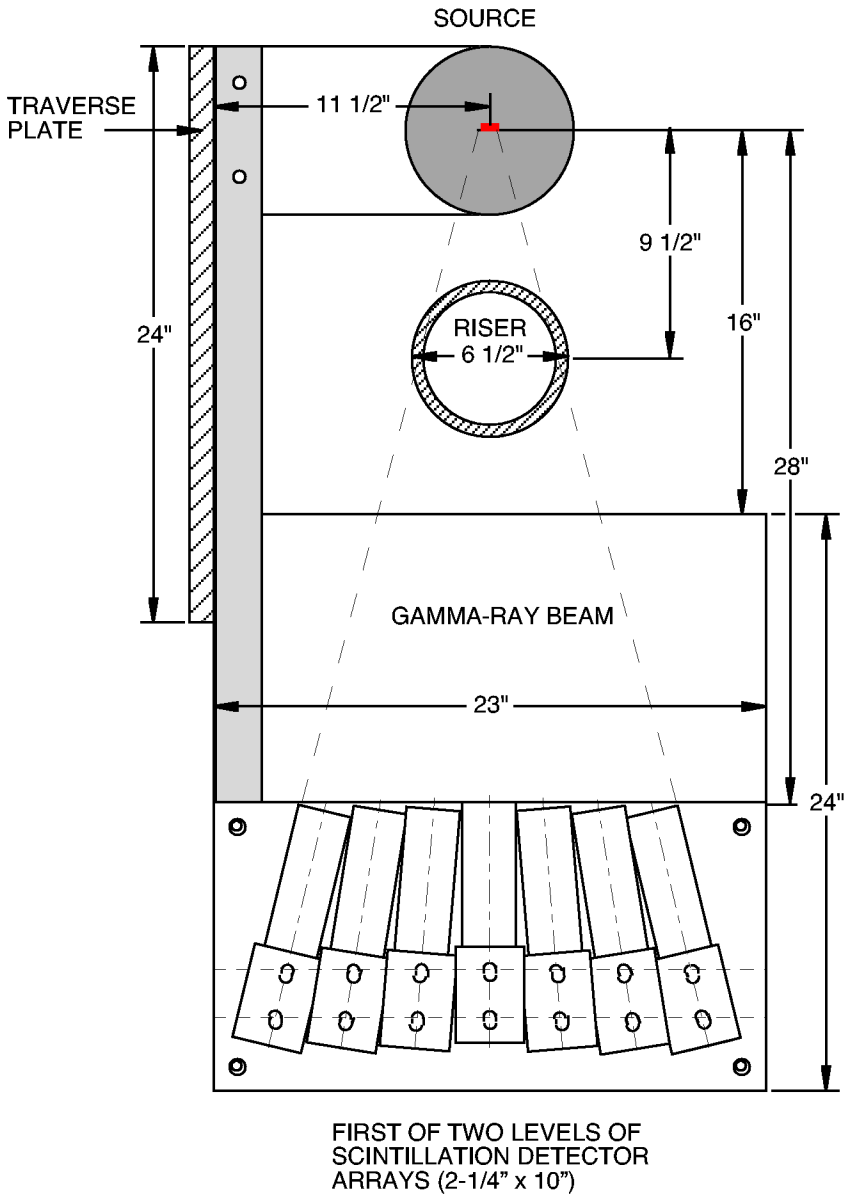

Figure 24 – Schematic of gamma-denstitometry tomography (GDT) system in the horizontal plane.

References

Cocco, R.A., Cleveland, J., Harner, R. and Chrisman, R. 1995 Simultaneous *in-situ* determination of particle loadings and velocities in a gaseous medium. In *Developments in Fluidization and Fluid Particle Systems, AIChE Symposium Series 308*, **91** J. Chen, H. Arastoopour, L.-S. Fan, D. King, A. Weimer and W.-C. Yang, eds. 147-153.

Coronella, C.J. and Deng, J. 1998 A novel method for isokinetic measurement of particle flux within the riser of a circulating fluidized bed. *Powder Technology* **99** 211-219.

Deng, J. 1997 Hydrodynamics of a cold circulating fluidized bed. *Ph.D. Dissertation.* The University of Nevada, Reno.

Geldart, D. 1973 Types of gas fluidization. *Powder Technology* **7** 285-292.

Harris, B.J. and Davidson, J.F. 1992 Velocity profiles, gas and solids, in fast fluidized beds. In *Fluidization VII, Proceedings of the 7th Engineering Foundation Conference on Fluidization*, Brisbane, Queensland, Australia, O.E. Potter and D.J. Nicklin, eds. Engineering Foundation, New York 219-226.

Issangya, A.S., Bai, D., Grace, J.R. and Zhu, J. 1998 Solids flux profiles in a high density circulating fluidized bed riser. In *Fluidization IX, Proceedings of the 9th Engineering Foundation Conference on Fluidization*, Durango, Colorado, USA, L.-S. Fan and T.M. Knowlton, eds. Engineering Foundation, New York 197-204.

Karri, S.B.R., Knowlton, T.M. and Litchfield, J. 1995 Increasing solids flow rates through a hybrid angled standpipe using a bypass line. In *Fluidization VIII, Proceedings of the 8th Engineering Foundation Conference on Fluidization*, Tours, France, J.-F. Large and C. Laguérie, eds. Engineering Foundation, New York 557-565.

Merrow, E.W. 1986 A quantitative assessment of R&D requirements for solids processing technology. *Rand Corporation Note R-3216-DOE/PSSP.*

Miller, A. and Gidaspow, D. 1992 Dense, vertical gas-solid flow in a pipe. *AIChE Journal* **38**(11) 1801-1815.

Nguyen, T., Nguyen, A. and Nieh, S. 1989 An improved isokinetic sampling probe for measuring local gas velocity and particle mass flux of gas-solid suspension flows. *Powder Technology*, **59** 183-189.

Reinhardt, B., Cordonnier, A. and Florent, P. 1999 Use of an isokinetic sampling probe: Results in a cyclone. *Powder Technology* **101** 81-90.

Rhodes, M.J. and Laussmann, P. 1992 A simple non-isokinetic sampling probe for dense suspensions. *Powder Technology* **70** 141-151.

Shollenberger, K.A., Torczynski, J.R., Adkins, D.R., O'Hern, T.J. and Jackson, N.B. 1997 Gamma-densitometry tomography of gas holdup spatial distribution in industrial-scale bubble columns. *Chemical Engineering Science* **52** 2037-2048.

Torczynski, J.R., O'Hern, T.J., Adkins, D.R., Jackson, N.B. and Shollenberger, K.A. 1997 *Advanced Tomographic Flow Diagnostics for Opaque Multiphase Fluids*. Report SAND 97-1176. Sandia National Laboratories, Albuquerque, NM.

van Breugel, J.W., Stein, J.J.M. and de Vries, R.J. 1969 Isokinetic sampling in a dense gas-solids stream. *Proceedings of the Institution of Mechanical Engineers* **184**(3c) 18-23.

Zhang, W., Johnsson, F. and Leckner, B. 1995 Fluid-dynamic boundary layers in CFB boilers. *Chemical Engineering Science* **50**(2) 201-210.

Zhou, J., Grace, J.R., Qin, S., Brereton, C.M.H., Lim, C.J. and Zhu, J. 1994 Voidage profiles in a circulating fluidized bed of square cross-section. *Chemical Engineering Science* **49**(19) 3217-3226.

DISTRIBUTION

1 Paul Scheihing
U. S. Department of Energy
Office of Industrial Technologies, EE-20
1000 Independence Ave. SW
Washington, DC 20585

1 Brian Valentine
U. S. Department of Energy
Office of Industrial Technologies, EE-20
1000 Independence Ave. SW
Washington, DC 20585-0121

1 Tyler Thompson
Cooperative Research
The Dow Chemical Company
1776 Building
Midland, MI 48674

1 Raymond A. Cocco
The Dow Chemical Company
1776 Building
Midland, MI 48674

1 C. Stuart Daw
Oak Ridge National Laboratory
PO Box 2008, MS8088
One Bethel Valley Rd
Oak Ridge, TN 37831-8088

1 Cloyd Beasley
Oak Ridge National Laboratory
PO Box 2009, MS6359
One Bethel Valley Rd
Oak Ridge, TN 37831-6359

1 Richard D. LaRoche
DuPont Engineering Technology
DuPont Engineering
1007 Market St. N6521
Wilmington, DE 19898

1 Bryan A. Kashiwa
Los Alamos National Laboratory
T-3, MS B216
Los Alamos, NM 87545

1 James Fort
Pacific Northwest National Laboratory
P. O. Box 999, MS K7-15
Richland, WA 99352

1 Susan J. Gelderbloom
Dow Corning Corporation
P.O. Box 995
Midland, MI 48686-0995

1 Paul H. Merz
Chevron Research and Technology Co.
100 Chevron Way, P.O. Box 1627
Richmond, CA 94802-0627

1 Thomas O'Brien
NETL, U.S. Department of Energy
P.O. Box 880, MS NO4
Morgantown, WV 26507-0880

1 Rutton D. Patel
Reactor & Fluid Dynamics Section
Exxon Research & Engineering Co.
180 Park Avenue
Florham Park, NJ 07932

1 James M. Tippett
Du Pont Central R&D/Materials Sci & Eng
P. O. Box 80356, Experimental Station
Wilmington, DE 19880-0356

1 Wen-Ching Yang
Siemens Westinghouse Power Corporation
Science and Technology Center
1310 Beulah Road
Pittsburgh, PA 15235-5098

1 Robert W. Lyczkowski
Argonne National Laboratory
Energy Systems Division
Bldg 362 Room C348D
9700 South Cass Avenue
Argonne, IL 60439-4831

1 Professor Muthanna Al-Dahhan
Department of Chemical Engineering
Washington University
One Brooking Drive, Campus Box
St. Louis, MO 63130-4899

1 Professor Steven Ceccio
Dept. of Mechanical Engineering
The University of Michigan
2043 W. E. Lay Automotive Laboratory
1231 Beal Ave.
Ann Arbor, MI 48109-2121

1 Professor Milorad Dudukovic
Department of Chemical Engineering
Washington University
One Brooking Drive, Campus Box 1198
St. Louis, MO 63130-4899

1 Professor Dimitri Gidaspow
Department of Chemical & Environmental Engineering
Illinois Institute of Technology
10 West 33rd Street
Chicago, IL 60616-3793

1 Yun Xiong
Millennium Inorganic Chemicals
6752 Bay Meadow Drive
Glen Burnie, MD 21060

1 Professor John B. McLaughlin
Department of Chemical
Clarkson University
Potsdam, NY 23699-5705

1 Professor William W. Schultz
Dept. of Mechanical Engineering
The University of Michigan
2027 W. E. Lay Automotive Laboratory
1231 Beal Ave.
Ann Arbor, MI 48109-2121

1 Professor Jennifer Sinclair
Department of Chemical Engineering
Purdue University
West Lafayette, IN 47907-1283

1 Professor Sankaran Sundaresan
Department of Chemical Engineering
Princeton University
A-315, Engineering Quadrangle
Princeton, NJ 08544

1 MS 0710 A. P. Sylwester, 6245
1 MS 0826 J. R. Torczynski, 9117
1 MS 0834 T. J. O'Hern, 9112
1 MS 0834 K. A. Shollenberger, 9112
1 MS 0834 S. M. Trujillo, 9112
1 MS 0834 A. C. Ratzel, 9110
1 MS 0834 T. W. Grasser, 9112
1 MS 0834 J. E. Johannes, 9114
1 MS 0834 Day File, 9112
1 MS 0841 T. C. Bickel, 9100
1 MS 0886 N. B. Jackson, 1812
1 MS 9018 Central Technical Files, 8945-1
2 MS 0899 Technical Library, 9616
1 MS 0612 Review and Approval Desk, 9612
For DOE/OSTI